SALT MARSH HYDROLOGY AND RESTORATION

A Dissertation

by

THOMAS PRESTON HUFF

Submitted to the Office of Graduate and Professional Studies of
Texas A&M University
in partial fulfillment of the requirements for the degree of

DOCTOR OF PHILOSOPHY

Chair of Committee,	Rusty A. Feagin
Committee Members,	Jens Figlus
	Roel Lopez
	Hsiao-Hsuan Wang
Head of Department,	Kathleen Kavanagh

August 2017

Major Subject: Ecosystem Science and Management

ABSTRACT

Hydrologic changes have affected coastal ecosystem sustainability along the Texas coast and throughout the Gulf of Mexico. Human utilization of coastal ecosystems has led to the alteration of tidal hydrology. These ecosystems are highly dynamic and are greatly affected by tidal fluctuations and restriction to hydrologic flow.

The main objective of this study was to understand the hydrologic effects of tides, hydrologic alterations, and subsequent restoration on salt marshes along the Texas coast. The selected study site was Magnolia Beach marsh in Matagorda Bay, approximately 10.5 kilometers southeast of Port Lavaca, Texas. The study also had three more specific objectives.

The first objective was to determine the cause of marsh loss observed since 1958. This was accomplished by a GIS analysis that identified over 62 hectares of marsh loss and a hydrologic analysis that identified a pair of tidal barriers. These barriers reduced the volume of water that could be exchanged between the salt marsh and Matagorda Bay. This intermittent connectivity resulted in the internal waters of the marsh becoming hypersaline.

The second objective was to measure the hydrologic response to tidal reconnection with the removal of the two barriers. This was accomplished through the creation of a STELLA computer model, a numerical inlet hydrology model, and a meta-analysis to predict barrier removal success. An analysis of water level and water velocity

before and after the barrier removal was used to quantify the success of the hydrologic reconnection.

The final objective was to create a tide prediction model to better estimate wind-driven tides. The current NOAA model has been effective to give astronomical tide movements, but is not capable of predicting wind driven tides. The Enhanced Tide Model resulted in a 13.34% average increase in tidal prediction accuracy across all NOAA tidal gauges in the Gulf of Mexico and the East coast of Florida. This tool could be used by the public, the shipping industry, and restoration planners to better understand tide dynamics in the Gulf of Mexico and abroad.

DEDICATION

This thesis is dedicated to my parents, Rhonda and Preston Huff, for personally seeing to my education through ten years of homeschooling. You gave me all the tools necessary to succeed at anything. Thank you.

ACKNOWLEDGEMENTS

I would like to deeply thank my committee chair, Dr. Rusty Feagin, and my committee members, Dr. Figlus, Dr. Lopez, and Dr. Wang. I have been honored to have your guidance and support in my academic career.

Thank you to all my friends, colleagues, and family that helped pushed me to always be my best. A special thanks to my friend and colleague, Arturo Delgado who was always willing to lend a helping hand in my research and never shied away when the work got tough.

I would also like to thank my family for their unwavering support and belief in me. Special thanks go to my sister, Hana, for her academic excellence that always challenged me to try and keep up.

Finally, I would like to thank my best friend and partner, Jess, for her patience and help throughout my college career.

CONTRIBUTORS AND FUNDING SOURCES

Contributors

This work was supervised by a thesis committee consisting of Dr. Rusty Feagin of the Department of Ecosystem Science and Management, Dr. Jens Figlus of the Department of Ocean Engineering, and Dr. Hsiao-Hsuan Wang and Dr. Roel Lopez of the Department of Wildlife and Fisheries Sciences.

All work for the thesis dissertation was completed by the student, in collaboration with Dr. Rusty Feagin of the Department of Ecosystem Science and Management.

Funding Sources

The Franklin F. Wasko Graduate Merit Fellowship provided partial support of this work, along with the Texas General Land Office Coastal Management Program Contract no. (14-086-000-7954), the Texas General Land Office Coastal Erosion Planning and Response Act Program under Contract no. (14-247-000-8344), the Mississippi-Alabama Sea Grant/National Oceanic and Atmospheric Administration Coastal Restoration Center Award Number (NA10NMF4630080, R/HRC-04), and Texas Sea Grant/ NOAA Award Number (NA14OAR4170102).

NOMENCLATURE

CTD	Conductivity, Temperature, and Depth
ETM	Enhanced Tide Model
mS	Millisiemens
ppt	Parts Per Thousand
GLO	General Land Office
CEPRA	Coastal Erosion Planning and Response Act
NOAA	National Oceanic and Atmospheric Administration
CPU	Central Processing Unit
RSLR	Relative Sea Level Rise
CIR	Color Infrared
b/w	Black and White
TC	True Color
TNRIS	Texas Natural Resources Information System

TABLE OF CONTENTS

Page

LIST OF FIGURES

Page

LIST OF TABLES

Page

CHAPTER I

INTRODUCTION

Land and water interfaces are some of the most valued landscapes globally (Costanza et al. 1997). Water access equates to economic value through increased housing prices, shipping, tourism, and outdoor recreation. This value places greater pressure on intercostal waterways and landscape types to provide ecosystem services for a plethora of uses (Feagin et al. 2015). Increased utilization subsequently results in greater related impacts to the landscape. Diking, dredging, wetland draining, and construction all alter the hydrology of the landscape and can lead to increased erosion, loss of coastal salt marshes, increased sediment transport, and altered tidal behavior (Bromberg, Silliman, and Bertness, 2009).

Humans have altered the coastal environment for centuries and as populations increase the utilization of coasts has increased. With climate change and the fluctuation of sea levels, the line between human infrastructure and water has grown thin. Coastal managers face increasing pressure to meet both human and environmental needs while planning for an increasingly dynamic environment (Feagin, 2015).

Land managers need to take a progressive approach to environmental restoration, and coastal protection. Effective coastal protection and management will continue to become more difficult as climate changes progress. Therefore, the immediate restoration of degraded marsh ecosystems through hydrologic restoration is crucial to preserve the ecosystem service value for fisheries and storm protection.

To support coastal planners and government officials to make coastal management decisions, we studied the success of barrier removal as an option for salt marsh restoration along the Texas Gulf Coast, and subsequent restoration of tidal connections. To further aid in the safe utilization of tidally connected waters, an Enhanced Tide Model was created to more effectively estimate wind driven tides. The work outlined above will fill a gap in current knowledge and create a framework for future restoration and public safety.

CHAPTER II

HYDROLOGIC BARRIERS AS A CAUSE FOR SALT MARSH LOSS

Introduction and Literature Review

Salt marshes are some of the most productive ecosystems in the world (Day et al., 1995). However, many of these environments have been hydrologically altered by humans and these alterations can affect their sustainability under future conditions, including changing drought periods or relative sea level rise (RSLR) (Bouma et al., 2014; Bromber, Silliman, and Bertness, 2009). This human interference can alter the species composition and result in reduced species richness (Kirwan et al., 2010; Mathews et al., 2014). As hydrology is modified, the health of the marsh plants, birds and fish using the area is also modified (Boesch and Turner, 1984; Broome, Seneca, and Woodhours, 1988; Day et al., 1995; Temmerman, De Vries, and Bouma, 2012).

Hydrological alternation can include drainage for agricultural usage (Portnoy, 1999; Roman et al., 2002; Tiner, 1984; Warren et al., 2002), the construction of canals by oil and gas exploration activities (Boesch and Turner, 1984; Ko and Day, 2004; Roman, Niering, and Warren, 1984), and mosquito diking (NOAA, 2010). Hydrological alterations can cause chemical changes within the marsh soil and water of the marsh ranging from decreased soil salinity levels in drained marsh soil to high salt levels in impounded salt marshes (Delgado et al., 2013; Portnoy, 1999). Impoundment and hydrological disconnection can contribute to increased subsidence (Turner and Neill,

1 *Reprinted with permission from "Hydrological barriers as a cause for salt marsh loss" by Huff and Feagin, 2017. Journal of Coastal Research, NO.77, pp. 88-96, Copyright [2017] by Journal of Coastal Research.

1983), reduce rates of sedimentary accretion and freshwater mixing (Colon-Rivera et al., 2012), and result in re-distribution of herbaceous species (Sinicrope et al., 1990).

Hydrological restoration includes the removal of barriers to tidal flow, and can be a productive method to reverse or reduce marsh loss (Firth et al., 2014; Turner and Neill, 1983). As shown by Warren et al. (2002), the re-introduction of tidal action can rehabilitate a former salt marsh in stages, with the vegetation closest to the restored tidal edge experiencing greater immediate recovery, although some marshes can still take up to 15 years for other functions to fully recover. Still, barrier removal can result in recovery over great areas, with only a small amount of cost and effort expended (NOAA, 2010; Sinicrope et al., 1990). As part of this increased emphasis by NOAA on the cost effectiveness of removing barriers as a manner of marsh restoration, we identified a large marsh complex that was suffering from hydrological disconnection. This marsh complex stretches from Magnolia Beach to Indianola, Texas.

Our primary objective was to quantify the amount of marsh loss, and ascertain if this loss was related to hydrological barriers. We measured data on land cover changes in the marsh complex from 1958 to 2012, and then related these changes to RSLR, precipitation, and barrier location. We also identified the magnitude of the barriers to present-day hydrology in terms of their effect on changing water levels and salinity. This was conducted via analyzing in-situ data to understand past differences. Using this approach, we show the potential for removing relatively small barriers as a cost-effective solution to counter-act marsh losses across broad areas of land.

Methods

Study Area

The study area is a complex of coastal salt marshes located on the west shore of Matagorda Bay near Indianola and Magnolia Beach, an area south of Port Lavaca, Texas (Figure 1). These marshes were historically connected to Matagorda Bay by at least two pathways; one natural inlet at the north end of the marsh known as Magnolia Inlet, and a second natural connection to the south that leads to Powderhorn Lake through an area known as Fish Pass.

The vegetation within the low (intertidal) marsh is characterized by *Spartina alterniflora*, with *Batis maritima* and *Salicornia virginica* dominant at slightly higher elevations or at more hydrologically distant portions of the marsh. The low marsh transitions to unvegetated salt flat as elevation increases. A small bluff exists in many portions of the area, where the salt flat quickly transitions into upland vegetation, composed primarily of Tamaulipan scrub with *Opuntia* sp. and *Yucca gloriosa* along the periphery of the wetlands. Large salt flats are common in the portions of the marsh south of Zimmerman Road (Figure 2).

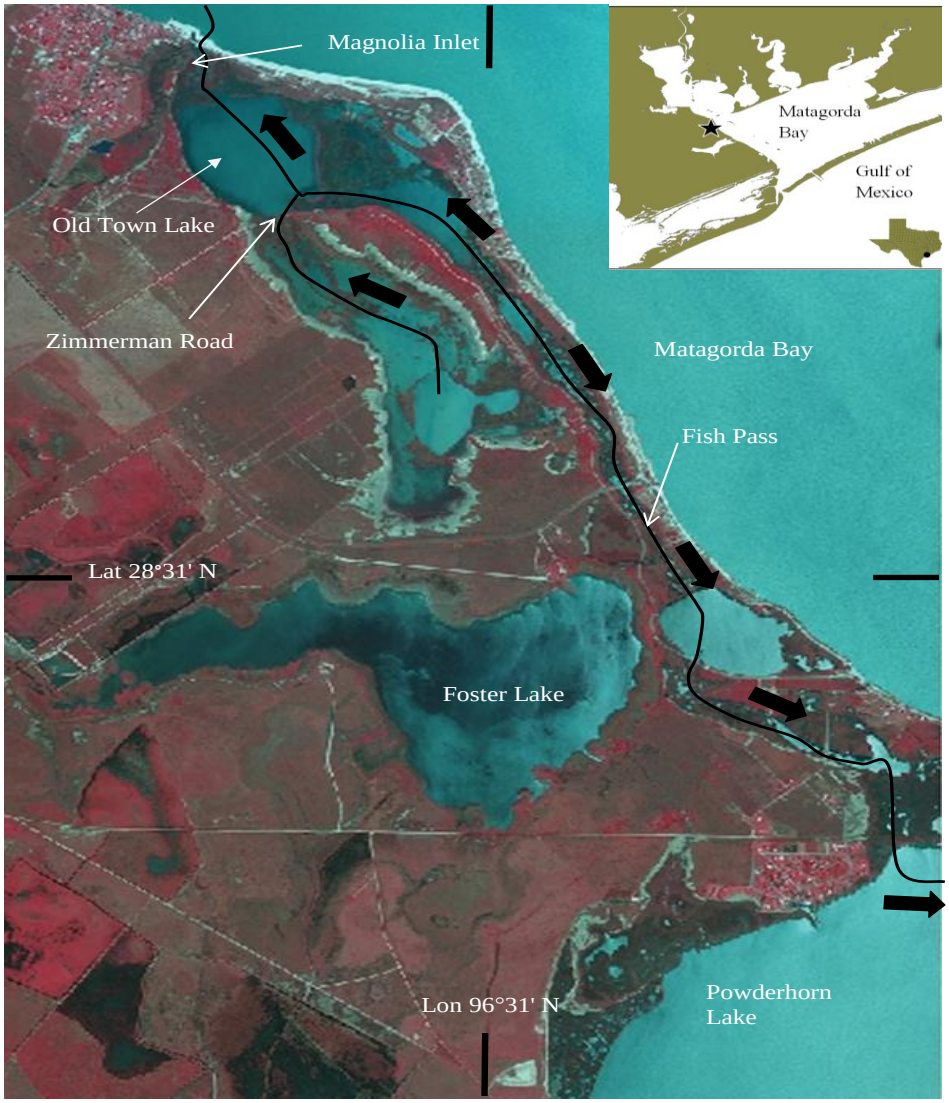

Figure 1: Research site location and surrounding water bodies with water connectivity shown with arrows.

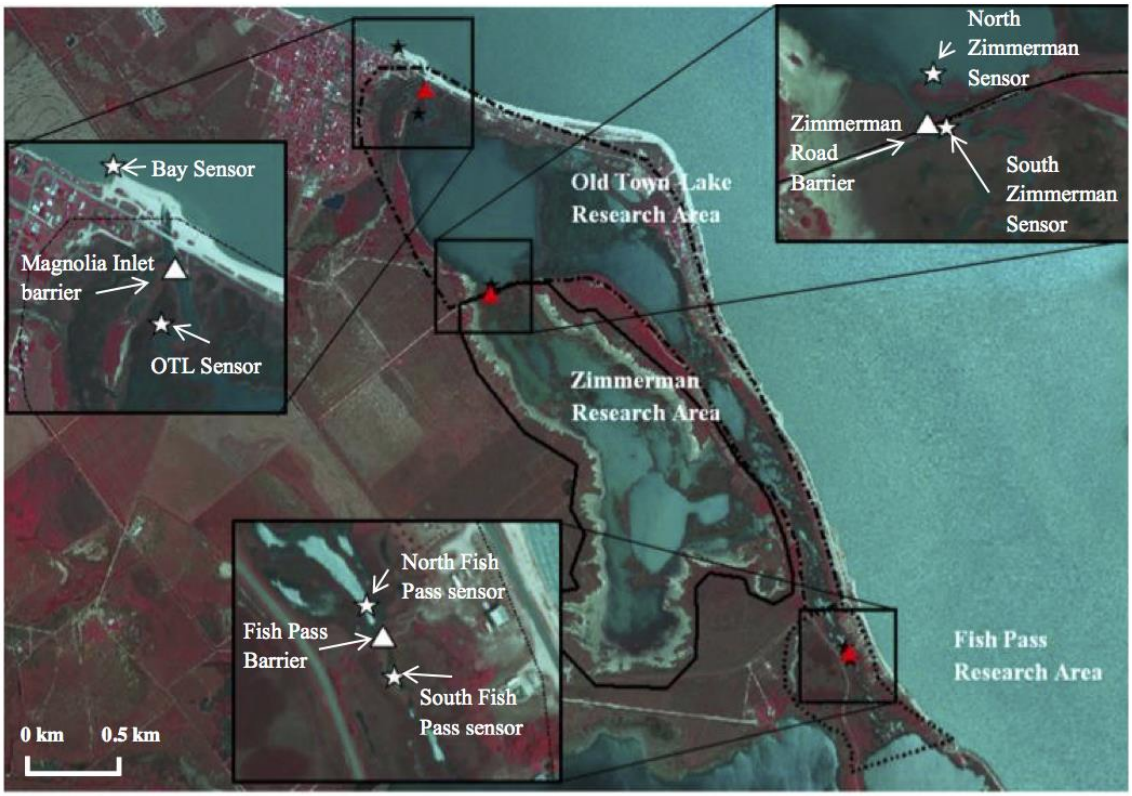

Figure 2: Research site with locations of blockages indicated with triangles and tidal gauge locations with stars. The lined areas indicate the marsh area.

Prior to this study, it was becoming increasingly apparent to residents and coastal managers that (while lacking quantitative data) the vegetation had been dying, nekton numbers were reduced, and marsh area was declining. The causes of the deterioration were not understood, but suspected to be due to hydrological barriers that block tidal flow. Three potential barriers were initially identified. The first barrier was a shell and mud debris pile spanning the width of Magnolia Inlet. This debris appeared to have accumulated to block the majority of the connection from Old Town Lake to Magnolia Bay. Another barrier existed at Fish Pass, and appeared to be a shell-hash road that stretched across the marsh surface constructed sometime prior to 1958 (Figure 2). This

barrier was removed on May 27, 2013. Another potential barrier existed at Zimmerman Road, which was a shell-hash road that stretched across the marsh, with construction prior to 1958. At Zimmerman Road, culverts were in place through a small gap in the road, though they appeared to be partially clogged with sediment.

Land Cover Analysis

A series of land cover maps were created ranging over the time period from 1958 to 2012, and compared for land cover changes (Figure 3). Aerial photos were obtained from the Texas Natural Resources Information System (TNRIS) over a range of five unique dates, with variable resolutions (1958, 0.5 m, b/w; 1979, 5 m, CIR; 1996, 1 m, CIR; 2002, 3.5 m, TC; 2012, 1 m, TC). The span of the images was chosen on the resolution and quality of the images to give a representative sequence of landscape changes over time. Any images possessing clouds or of greater than 5 m resolution were not considered. SPOT satellite panchromatic images (April 1991, April 1992, April 1993, all at 30 m) were also obtained from TNRIS.

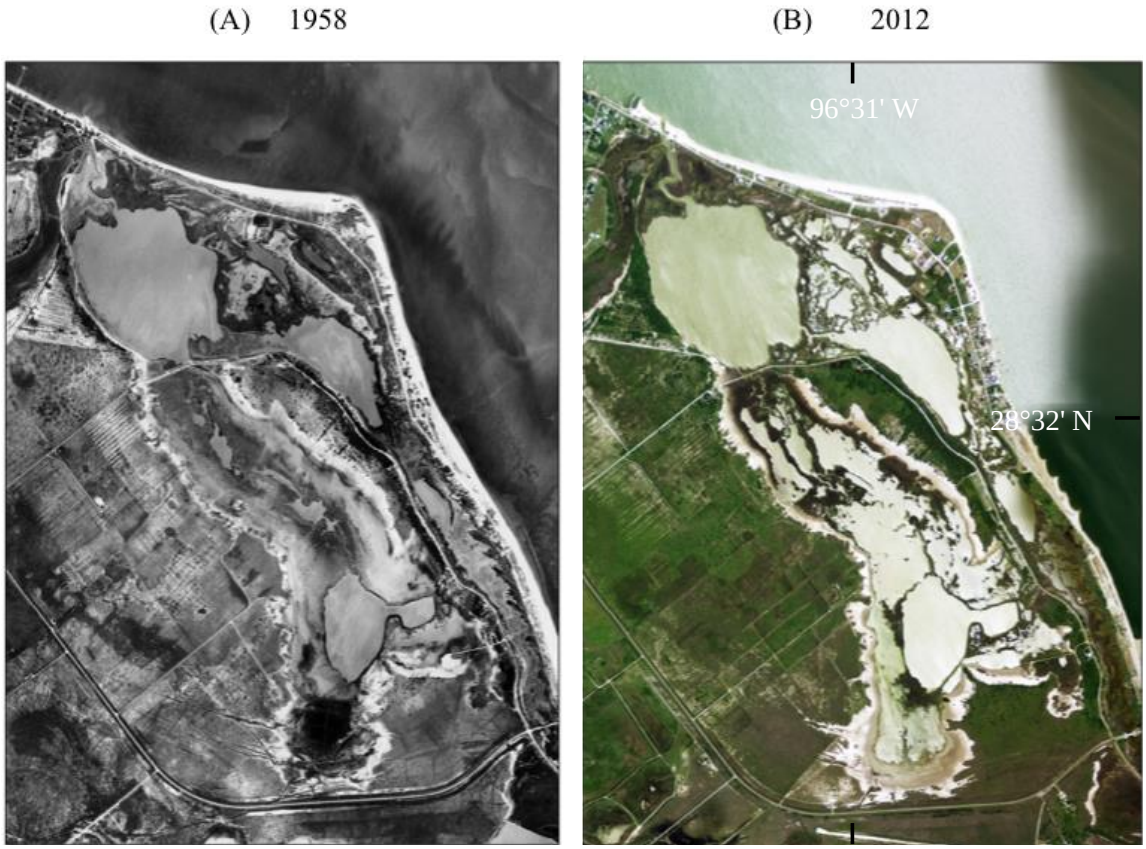

Figure 3: Figures (A, B) denote the time frame used as a comparison of land cover change overtime ranging from 1958 to 2012. Courtesy of TNRIS.

Within a GIS (ArcGIS 10.1, ESRI), three different land cover classes (water, low marsh, and salt flats) were hand digitized at a consistent view scale of 1:2000. This digitization was double-checked by a second researcher who reconciled any differences that existed in landscape classifications over the span of years. Next, the total area of each land cover type was calculated in m^2, and converted into a percentage of total landscape for comparison. Area calculations were conducted for the total marsh complex from the area immediately surrounding Fish Pass to Magnolia Inlet, and still including the Zimmerman Road marsh.

An accuracy assessment was subsequently conducted on the digitization effort for the 2012 image. A total of 50 points were sampled in the field using a hand-held Trimble GPS unit, with each point taken within at least 15 meters of the edge of two intersecting land cover boundaries. At each point in the field, the true land cover was recorded and then compared to the 2012 classified cover type. The accuracy of the effort was 69.93 % for the entirety of the study area. However, most of this error was attributed to two sampling locations, Fish Pass (55.88% accuracy), and the south end of the Zimmerman Road marsh (44.12% accuracy), where water was misclassified as salt flats, and vice-versa. This source of error was due to the fact that large expanses of salt flats are often covered with water, depending on the amount of rainfall, tides, runoff, etc., in these two portions of the marsh complex. The Magnolia Inlet portion of the complex had a total accuracy of 96.67% along with the area at the south end of Old Town Lake just north of Zimmerman Road with 83.02% total accuracy. These two areas contained less salt flat which was the most stochastic landscape class, and thus resulted in much higher accuracies.

The only way to reduce error in this method was to do the classification by hand. An unsupervised or supervised classification was not used due to the error within the process itself. The most accurate method we could use was to classify the image by hand digitization. This reduced the error of other automated methods, however, the error was still high due to the dynamic nature of a salt marsh. Tides allow for salt flats to be flooded within hours, and are thus classified as water instead of salt flats. Higher

temporal resolution imagery could help alleviate this issue, but currently this imagery doesn't exist. We were limited to NAIP imagery with a temporal resolution of 2 years.

While this was the most accurate method, additional errors could exist in the use of different color imagery, different resolutions, and user interpretation of land cover classes. Utilizing the highest resolution imagery and hand digitization are the only methods that could help rectify these errors.

Hydrologic Analysis

Monthly average precipitation was obtained from the Port Comfort weather station in Port Comfort, Texas (#ID GHCND: USC00417140, 10.87 km away from study area) over a date range from 1957 to 2013. Hourly Precipitation data was obtained from a Palacios, Texas based land weather station (Station COOP: 416750). This was matched to the tidal gauge data time frame (March 26, 2013 to August 29, 2013). Monthly relative sea level was obtained from the National Oceanic and Atmospheric Administration (NOAA) buoy located in Rockport, Texas (#ID 8774770, 77.71 km away from study area) over a date range from 1948 to 2012. Moving averages were calculated on both data sets within a window of 12 months, and were subsequently graphed (Dunton, Hardegree, and Whitledge, 2001). The precipitation and sea level over specified date ranges were plotted and linearly regressed against time, in order to calculate rates of change (as measured by a linear slope, with the goodness-of-fit measured by r^2). The dates of the classified aerial imagery were used as bounding dates for each calculation.

Water level and conductivity were measured every hour from March 26, 2013 to August 29, 2013, using CTD gauges (CTD-Diver, Schlumberger) placed on opposing sides of the three barriers of interest (Figure 2). Gauges were suspended on fishing line, within 3/4-inch diameter PVC pipes that were set vertically within the water column. The top of each PVC pipe was surveyed using survey-grade GNSS system composed of a Trimble R8 receiver, using the Fast Static method (average RMS=0.002 m, average horizontal precision=0.008 m, average vertical precision=0.012 m).

Gauge depth readings were subsequently converted into vertical NAVD88 units and graphed. Due to the slight errors in the GNSS height measurements, the data were matched for gauges on the opposing sides of barriers, using the high-water mark on May 29, 2013 at 16:00 as the reference date, for the Fish Pass and Zimmerman Road locations only. Finally, the outliers in the conductivity measurements were removed from the dataset for the Bay and North Fish Pass sensors. Values below 30 mS were removed from the bay values, and everything below 60 mS was removed from the North Fish Pass dataset. Negative data spikes were visible below these values and were filtered out using the data limits listed above.

Results

The land cover arrangement in the marsh was highly dependent on elevation above water level. Water occupied the lowest areas, with low marsh next ringing the water's edge or areas that experienced periodic tidal inundation. Salt flats followed as one moves up in elevation, with an upland scarp above them (Figure 4).

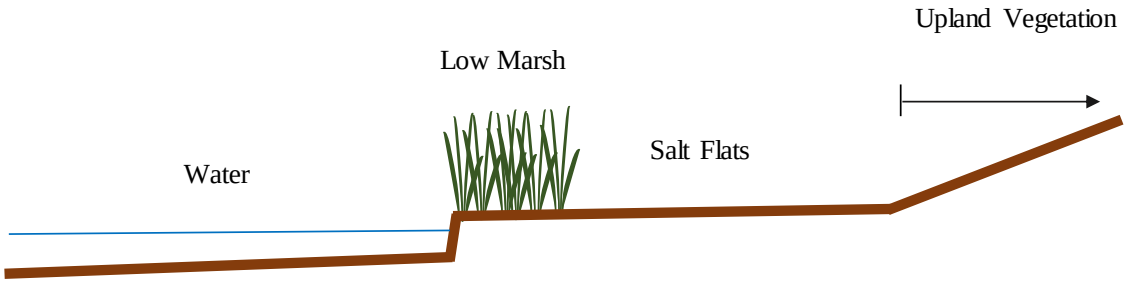

Figure 4: The land cover is influenced highly by elevation. Water at the lowest areas, followed by low marsh, then salt flats and finally a quick transition to upland vegetation.

Low marsh area decreased overall from 1958 to 2012 within the marsh complex (Figure 5A; Figure 3). Salt flats also decreased, and water increased. Low marsh and water were inversely related, in general. The period from 1958 to 1979 appeared to be an aberration to the general trend, with low marsh increasing quite strongly. The same trend was found for the areas bounded within each barrier (Figure 5B-D). The Magnolia Inlet area experienced the most drastic decrease in salt flat area when compared to the other regions within the marsh from the time period of 1958 to 1979.

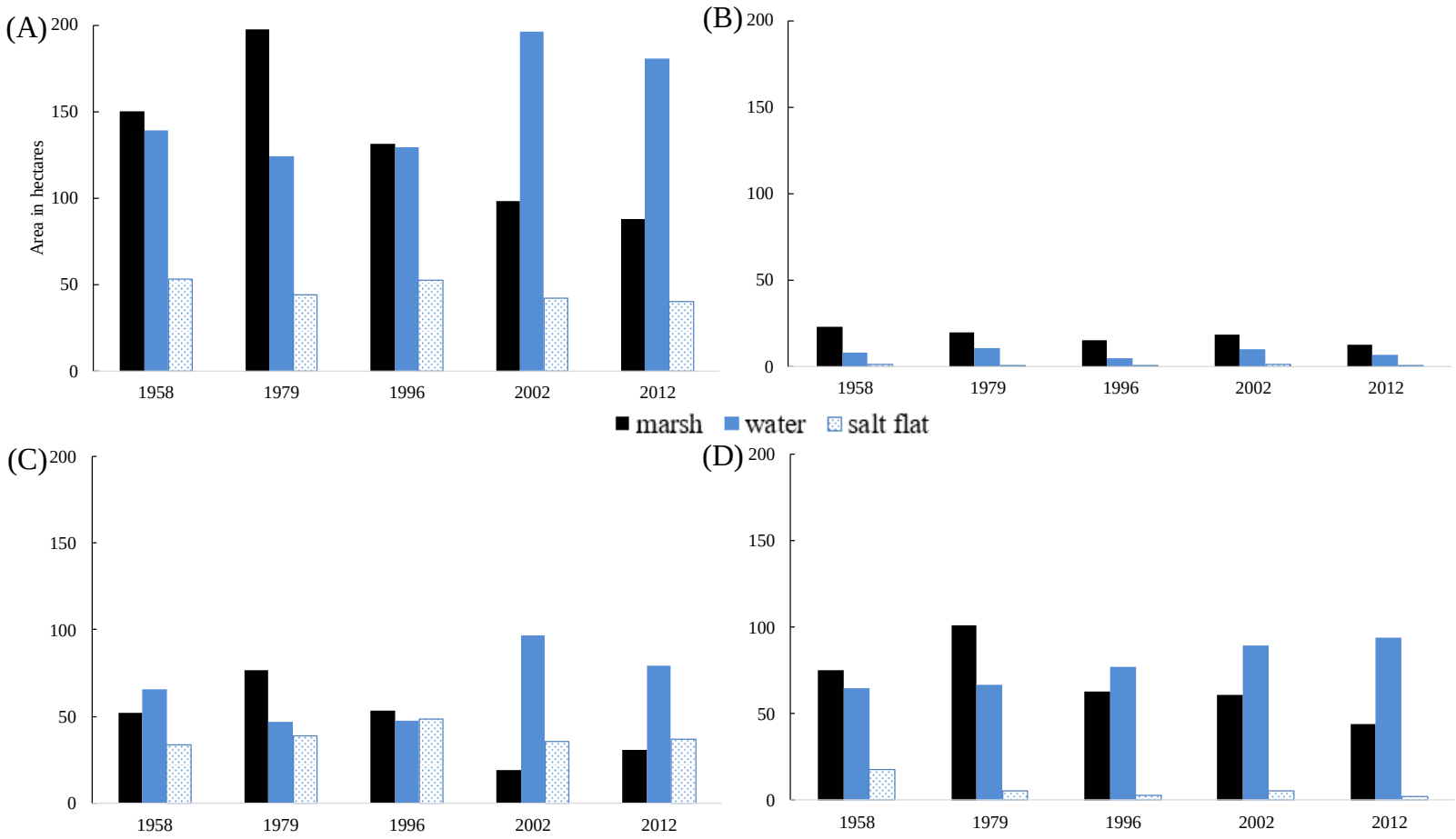

Figure 5: Land cover changes for 1958, 1979, 1996, 2002, and 2012 listed in square kilometers: total area of the marsh complex (A), and impounded areas lying behind the barriers at Fish Pass (B), Zimmerman Road (C), and Magnolia Inlet (minus those areas also behind Fish Pass and Zimmerman Road) (D).

When visually assessed in our data set, it was apparent that this salt flat in Magnolia Inlet had been converted to low marsh. This low marsh area was then subsequently lost between 1979 and 1996, converting to open water (Figure 5D).

A major low marsh loss event in the Zimmerman Road portion of the marsh complex visually appears to have occurred between 1991 and 1993, as recorded by the SPOT imagery. A linear regression was performed on the rainfall and relative sea level rise data from 1958 to 2012. Subsidence was incorporated into the relative sea level measurement. Over the entire period from 1957 to 2013, there was a noticeable decrease in the precipitation and an increase in relative sea level rise rate (Figure 6; Table 1). During this period, the sea level rose an average of 5.342 mm per year (r^2=0.8397, p-value = < 0.000) and the rainfall decreased at a rate of 0.832 mm/yr. (r^2=0.02532, p-value = 0.1229). After 1996, there was a rapid period of change in sea level rise. During the period from 1996 to 2002, the sea level increased on average at 16.74 mm per year. During the subsequent period from 2002 to 2012, the sea level rise rate was at its lowest (2.77 mm per year), while precipitation greatly decreased during this time frame (-0.832 mm/year).

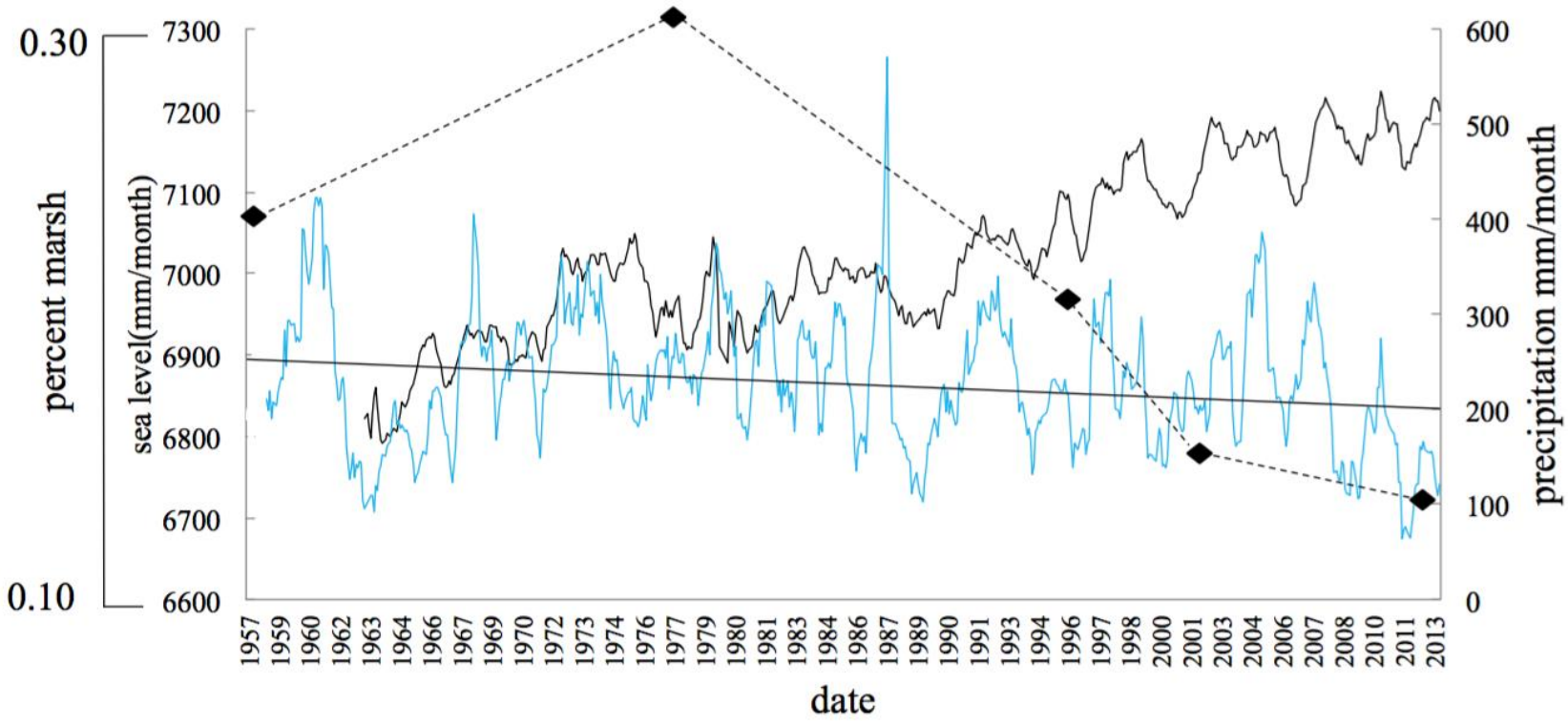

Figure 6: Monthly precipitation and sea level plotted against percent marsh area. The blue line denotes a 12-month moving average for precipitation. The black line denotes a 12-month moving average for sea level rise. The black dashed line indicates the percent low marsh within the study area as compared to the other landscape classes.

Table 1: Sea level rise rate, precipitation change, and precipitation averages over time frames of interest.

date	Slope sea Level (mm/month)	r^2	slope precip (mm/month)	r^2	precipitation averages (mm/month)
1958-1979	0.8815	0.1512	0.0851	0.00004	238.10468
1979-1996	0.6063	0.0974	-0.2472	0.0044	236.7637188
1996-2002	1.0245	0.0367	-0.0503	0.00003	214.8487222
2002-2012	0.231	0.0071	-1.1531	0.0431	207.8296303
Overall	0.5257	0.4145	-0.0778	0.0053	229.0516

Precipitation during tidal gauge sensor deployment shows that there was little correlation between salinity, response and rainfall. The drop in salinity was due to tidal infiltration. Reductions in salinity independent of precipitation, indicate bay water exchange can lower the salinity throughout the system (Figure 7).

Wind direction and velocity play a strong role in controlling the tidal action within Matagorda Bay (Figure 8A). Old Town Lake is hydrologically disconnected from Matagorda Bay for much of the year, and has an average water level of 38.20 cm with a standard deviation of 7.18 cm as compared to 30.61cm and 14.79 cm respectively in the open bay (Figure 8B). For weeks at a time (for example June 9, 2013 to June 24, 2013), Old Town Lake appears to be evaporating, with no connection to the sea. In contrast, Zimmerman Road is not currently limiting tidal exchange as evidenced by the gauges at North Zimmerman and South Zimmerman (Figure 8C). Still, the general trends and the evaporative time periods match those in Old Town Lake, indicating that these locations are suffering from the same barrier as Old Town Lake.

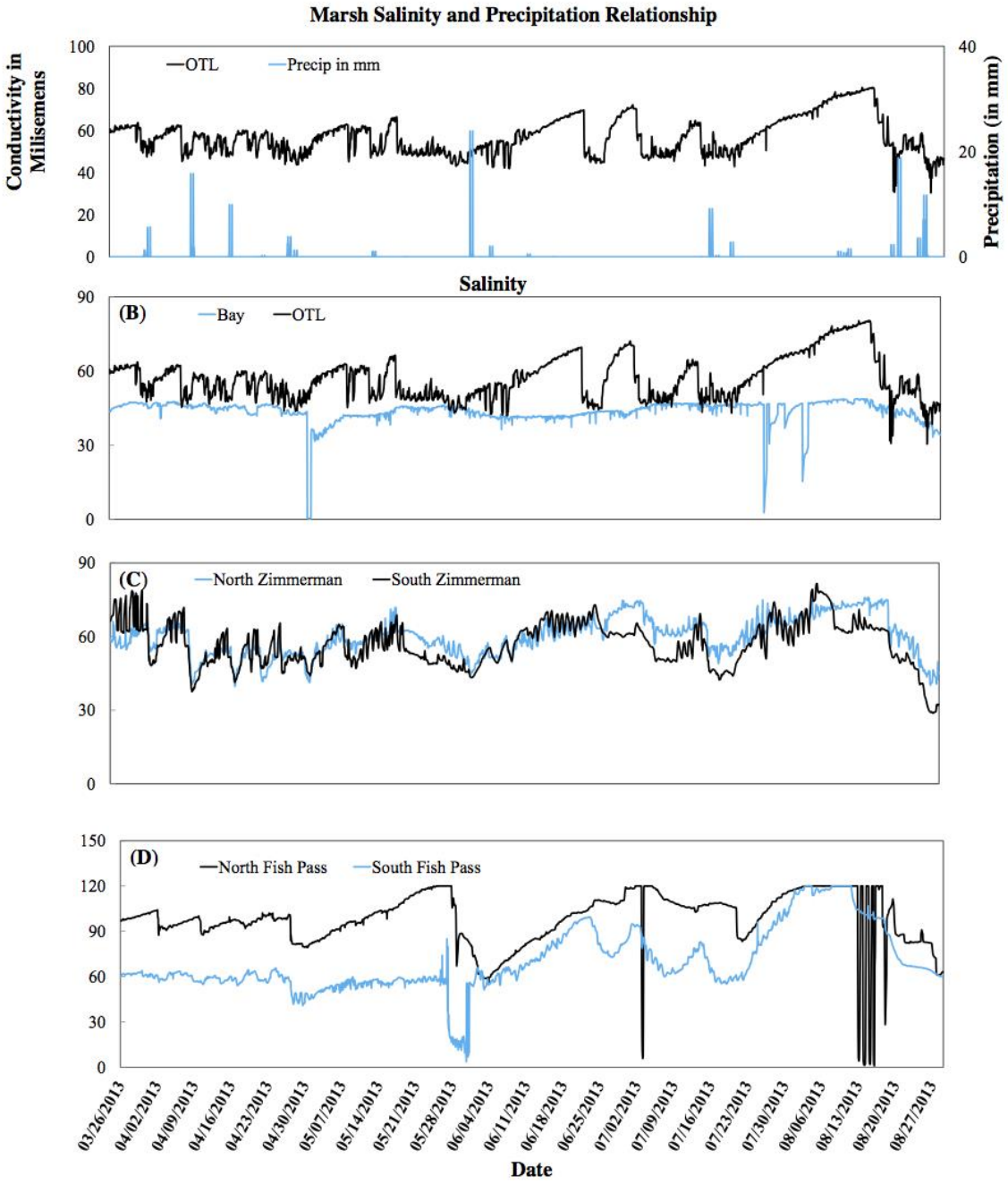

Figure 7: Salinity of Old Town Lake (OTL) compared to rainfall events from March 2013 to August 2013. The black line indicates the OTL salinity in millisiemens and the blue bar shows rainfall events in mm. Figures (B-D) show the comparison of salinity on opposite sides of the suspected barriers without the inclusion of rainfall data.

The barrier at Fish Pass presents a moderate hydrological barrier, as evidenced by the gauges at North Fish Pass and South Fish Pass (Figure 8D). On May 7, 2013, a strong NW wind was observed (likely a cold front) which caused one of the lowest recorded water levels within the marsh. The connectivity between South Fish Pass and Powerhorn Lake is evident in the degree to which the water levels fluctuate based on wind direction. In this case on May 7, 2013 the water was pushed to the south and away from the South Fish Pass sensors. The opposite function is occurring in North Fish Pass where you can see the gathering of water (55.49 cm in depth) in the same time frame that South Fish Pass can be observed to be draining (15.89 cm in depth). This indicates a reduced hydrologic exchange and in this case, there was no hydrologic exchange. This wind driven water movement can be seen in the same time frame in the Old Town Lake data along with the Bay data. A simple regression model was performed that produced an r^2 of 0.4182 (p-value < 0.0001). However, there is less change regarding the Zimmerman Road sensors due to the location ($r^2 = 0.6538$) (p-value < 0.0001). There is no exit for the water to the south for this location and thus less water movement occurs during a cold front event than in the south Fish Pass and Old Town Lake locations. Fish pass indicated a similar level of correlation to that of Zimmerman Road with an r^2 of 0.6409 (p-value < 0.0001).

Precipitation, evaporation, or tidal flow connectivity may each play a role in controlling the conductivity (as a proxy for salinity) within Old Town Lake (Figure 7A). Over the course of the year, the average conductivity in Old Town Lake (56.98 mS) was much greater than that in Matagorda Bay (44.03 mS). Moreover, Old Town Lake

exhibited more considerable fluctuations (range of 49.996 mS) compared with Matagorda Bay (range of 18.16 mS). Increases in salinity are observed throughout the summer months for Old Town Lake, and are obvious on June 18, 2013 in Figure 7. Conductivity fluctuations were similar between North Zimmerman and South Zimmerman (Figure 7C), with their averages (59.96 mS, 57.06 mS, respectively) similar to that in Old Town Lake (56.98 mS). North Fish Pass and South Fish Pass (Figure 7D) followed similar temporal patterns in the first portion of the record prior to May 27, 2013, though at different averages (96.77 mS, 59.89 mS, respectively). In the second portion of the record conductivity was 100.40 mS and 72.84 mS for North Fish Pass and South Fish Pass respectively.

Discussion

Overall, there was a large loss of low marsh from 1958 to 2012. As the low marsh retreated, it was generally replaced by water. However, there was an increase in overall marsh vegetation between the 1958's and 1979's. Yet, this marsh was lost between 1979 and the 1996, returning the marsh to a vegetation level comparable to 1958. However, the marsh loss trend continued from 1979 to the present-day.

The loss of the low marsh vegetation is likely correlated with the high salinity levels within the marsh (Figure 5 & 7). Mostly this low marsh is occupied by *Spartina alterniflora*, which has difficulty persisting when salinity levels are higher than 325 mol m-3 NaCl (approximately 37mS) (Adams and Bate, 1995; Naidoo, McKee, and Mendelssohn, 1992).

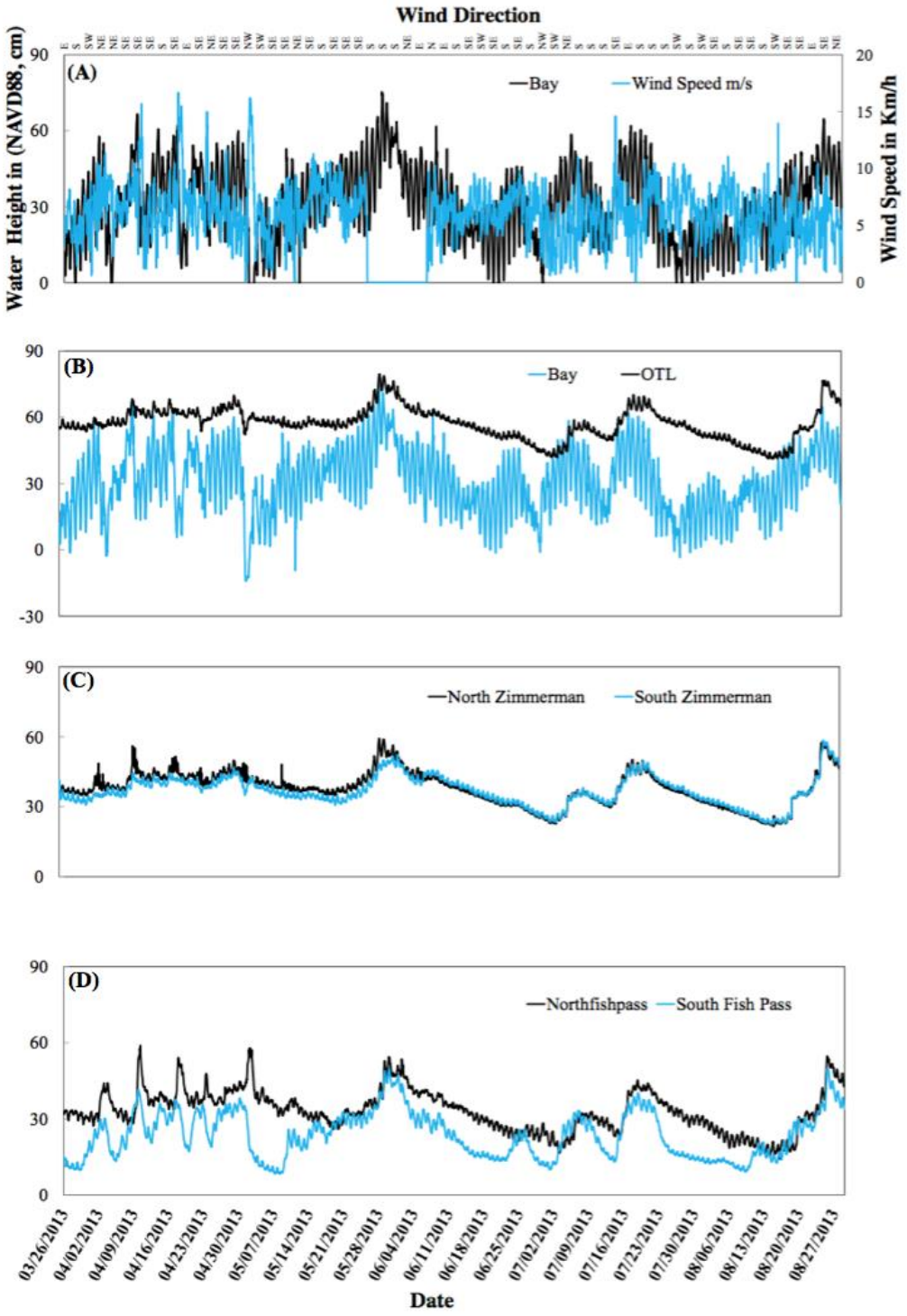

Figure 8: Local wind speed and direction, and water level in the open bay adjacent to the marsh (OTL) (A). Water level fluctuations on opposing sides of each suspected barrier (B-D).

Our records show salinities above this value most of the time in Old Town Lake and the rest of the marsh, but also show salinities reaching up to 120 mS particularly in the portions of the marsh with the most loss, such as North Fish Pass. In particular, evaporation occurs in the summer during high temperatures, and this worsens the conditions for vegetation and nekton. The result is the low marsh is converted to open water.

Many salt flats converted into low marsh between 1958 and 1979 in the Magnolia Inlet portion of the study area, resulting in a large increase in low marsh in 1979. Similar conversion of salt flats along the Central Texas Coast has been attributed to subsidence as caused by extensive hydrocarbon extraction activities during the 1950-1979-time period (White et al., 2006).

However, between 1979 and 1996 the marsh areas experienced a decrease of approximately 10% in total area throughout. This change was a conversion from low marsh to open water. This region was experiencing further subsidence, reduced rainfall, or a blockage to normal hydrological functions. During this time frame, there was not a large increase in relative sea level. While there was a general decrease in rainfall, there was not a significant change (-0.832 mm of precipitation a year). This suggests that the shell and mud debris pile reached a critical height and began to separate the marsh from the bay. This is confirmed by the local knowledge that the debris pile grew extensively in the 1990's. The SPOT image analysis indicates that the change occurred in 1992 and was solidified in 1993. This growth in the debris pile formed a dam that reduced the

frequency of tides that are capable of over topping the debris pile and infiltrating the marsh. Thus, water infiltration only occurs at higher tides. When these tides retreat, the volume of water held within the marsh is larger than historic volumes as the water ceases to exfiltrate the marsh. This would negatively affect the marsh in two key ways. The first being extended periods of low marsh flooding, and the second being hyper salinity through water evaporation. The first factor would result in systematic retreat of the low marsh as the volume of water increased as the debris pile grew. This process would be compounded with increased salinity within the marsh.

Therefore, the loss of low marsh area and the conversion of this area to open water can be directly attributed to the hydrologic barrier. Much of the marsh loss area was in secluded portions of the marsh and not directly exposed to wave energy. Thus, wave erosion can be eliminated as a driving factor of marsh loss.

The data show that the long-term trends of sea-level rise along with precipitation are not the driving factors in marsh loss. In addition, the marsh was unable to fully experience tidal fluctuations as visible in the tidal record. This indicates a barrier to water flow. This conclusion was supported by the salinity data, with water salinity inside the marsh only decreasing upon very high tides. With high water levels and hypersaline conditions observable for much of the sample period, the hydrologic barrier can be directly attributed to the marsh loss.

Conclusion

To begin the reversal of the marsh loss process, the past hydrologic processes must be restored. It was determined that the structure responsible for the modified

hydrology was the shell and mud debris in Magnolia Inlet. Channelization of the shell and mud debris pile could improve the tidal action within the marsh and alleviate the elevated salinity levels. The connection will also allow for greater volumes of water to be exchanged, thus helping to more completely mix the vast volume of water. The improved exchange volume reduces the possibility of hypersalinity and improves oxygenation of the water column. If incomplete mixing occurred between the marsh and bay waters, then salinity levels would not equilibrate. Therefore, further work was needed to identify how much of the barrier needed to be removed to restore hydrologic equilibrium.

CHAPTER III

RESTORING TIDAL EQUILIBRIUM: REMOVING A HYDROLOGIC BARRIER AND LOWERING SALINITY AT THE MAGNOLIA INLET, TEXAS

Introduction and Literature Review

Coastal salt marshes are dependent on periodic tidal inundation to restore salinity levels, allow for nutrient exchange, and permit aquatic species passage. When a hydrologic barrier blocks tidal flow, and impounds a body of water in a particularly hot or dry region, the salinity levels can increase as evaporation removes water (Delgado et al., 2013). If these conditions occur for extended periods of time, vegetation dies in these hypersaline waters (Portnoy, 1999). Nekton such as fish and shrimp become unable to leave or enter the system and populations suffer (Boesch and Turner, 1984).

The exchange of water is needed to flush out hypersaline water from within the wetland (Day et al., 1995). Salinity levels increase until lower salinity water can enter the system, whether from rainfall, runoff, or relatively less-saline estuarine bay water. If the disconnection continues for enough time, the salinity can reach toxic levels, causing fish kills and vegetation death.

Tidal marshes dominated by species such as Smooth cordgrass *Spartina alterniflora* reside in a compressed vertical arrangement, and this spatial context creates vulnerability to changes in relative water level. Altered water levels cause vegetative

2 *Reprinted with permission from "Restoring Tidal Equilibrium: Removing a Hydrologic Barrier and Lowering Salinity at the Magnolia Inlet, Texas" by Huff and Feagin, 2017. Journal of Coastal Research, NO.77, pp. 97-103, Copyright [2017] by Journal of Coastal Research.

retreat by modifying existing niches (Roman et al., 1984). Moreover, tidal marshes are highly influenced by the cyclical tidal inflow and retreat that drives the exchange of nutrients (Burkett and Kusler, 2000; Portnoy, 1999). A frequent supply of nutrients is needed for the vegetative communities along with the different aquatic species developing in the hatchery.

Hydrologic blockage was the catalyst for marsh and nekton loss at a complex of marshes between Magnolia Beach and Indianola, Texas (Figure 9). In this area, the tidal marsh is co-dominated by *Spartina alterniflora, Batis maritima,* and *Salicornia virginica* and though these species can tolerate relatively high salinity levels, the salinity in this marsh spiked as high as 120 mS (~90 ppt). Details on the salinities and the history of marsh loss at this location can be found in Huff and Feagin (2017).

The most feasible solution to restoring the marsh was the removal of the tidal barrier by mechanical means. As any removal was inherently destructive with the large construction machinery involved, a way to reduce the overall footprint of the excavation, while maximizing the environmental benefits was sought.

The overall objective in this study was to quantify and predictively model the channel cross section needed to hydrologically reconnect a marsh complex by both reestablishing tidal and salinity equilibrium with Matagorda Bay, Texas, and then verify the models using empirical data gathered after the barrier was removed.

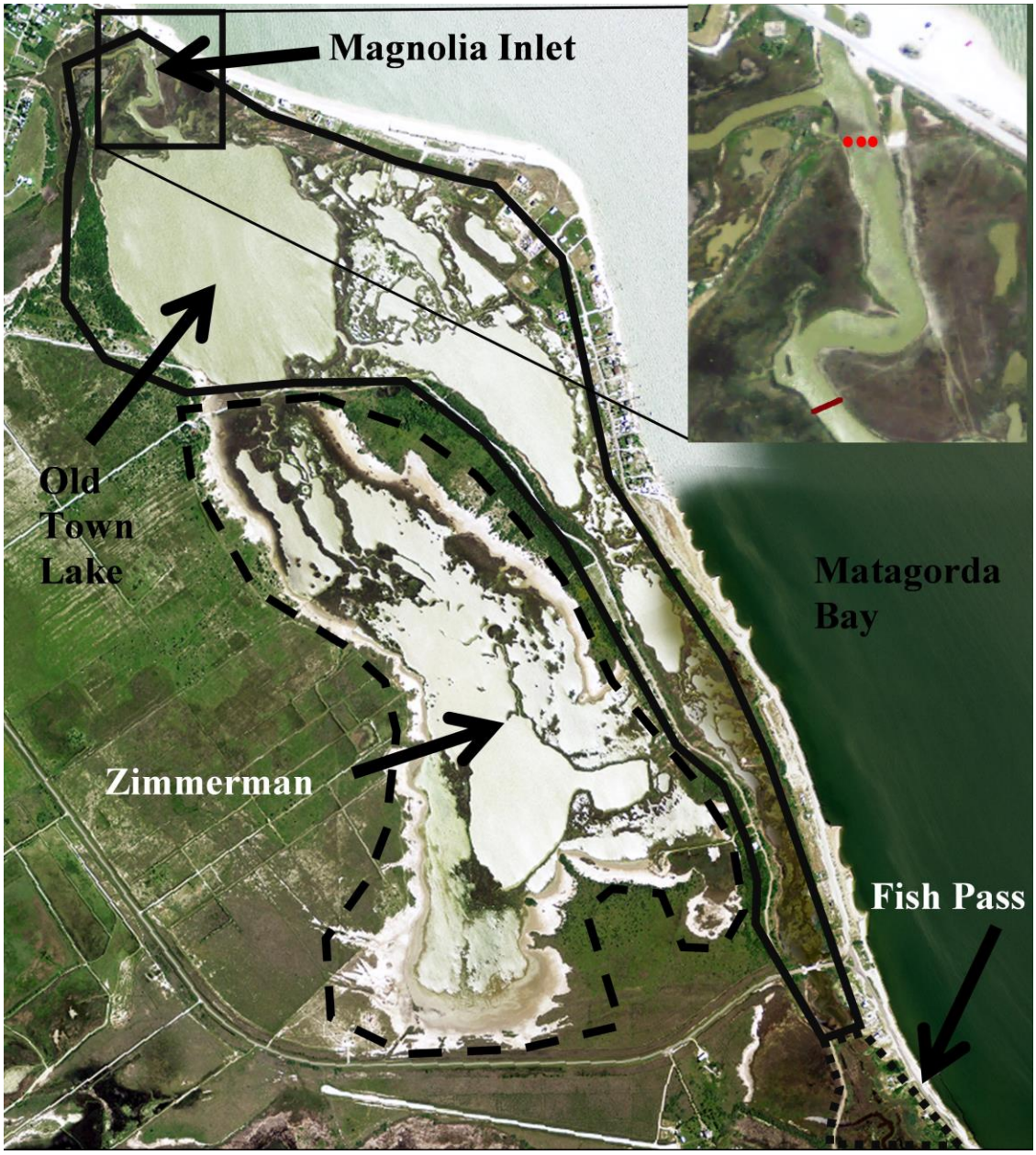

Figure 9: The study area with the three water bodies denoted in the polygons. Magnolia Inlet water body with the solid outline, Zimmerman Road water body with long dashes, and the northern extent of Fish Pass water body with the dotted line. The exploded view shows the location of the channel width transect (red line) and the core sampling points (red dots).

Specific objectives were to:

1. Calculate the cross-sectional area of the channel that would be required to restore exchange of the maximum tidal prism.
2. Identify the length of time necessary to equilibrate salinity once the hydrological flow was restored.
3. Quantify the volume of debris that would need to be removed to restore the flow.
4. Verify model values with in-situ data collected before and after barrier removal.

Methods

To accomplish the objectives, the study was split into four different sections. The first focused on the ideal cross section to allow for proper hydrologic exchange, the second on understanding the salinity exchange, the third on the barrier itself, and the fourth on confirmation of the modeled values

The main conceptual model is a hydrologic model that incorporates a numerical and meta-analysis that determines the cross section that is necessary to restore tidal equilibrium between Matagorda Bay and Magnolia Beach Marsh (Figure 10). The second model answers, assuming that complete connectivity was established, how long will it take for the salinity to equalize between the marsh and the bay. The third portion of the model is to look at the relationship between channel width and the water area within the marsh.

Numerical Model for the Ideal Cross-Section of Removal

To calculate the cross-sectional area of the channel that would be required to restore hydrological flow, a numerical model was developed, populated with empirical data from the study site (spring tide range, and water surface area), and then modeled to produce an ideal cross section. The numerical model was composed of two basic equations. A well-known relationship exists between the ideal cross-section of an inlet and the tidal prism of an internal body of water:

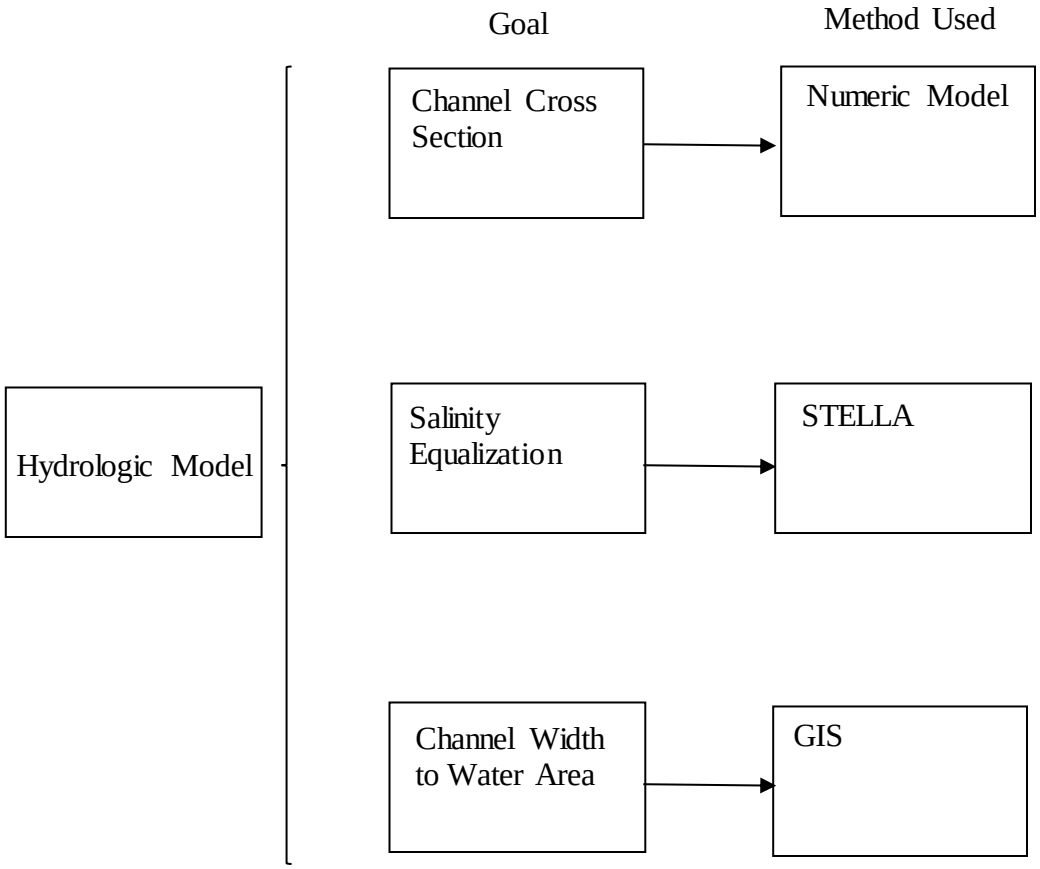

Figure10: Conceptual Hydrologic Model. This graphic outlines the use and flow of the different portions of the model and the tools used to complete each step.

$$A=aPm \qquad \text{Eq. 1}$$

Where A is the inlet cross-section in m^2, a is empirically-derived co-efficient, P is the tidal prism in m^3, and m is an empirically-derived power function. The maximum tidal prism P can be calculated by multiplying the surface area of a body of water, by the maximum spring tidal range. Values for a and m vary somewhat in the literature, depending on author and study location (Jarrett, 1976; Byrne et al., 1980; Powell, 2006, and Stive & Rakhorst 2008); much variation is due to the basin and inlet size, geography, and geomorphic context. An average of a ($5.21 * 10^{-3}$) and m (0.784) values were gathered from the literature. The maximum value for a was found to be $9.902 * 10^{-3}$ and a minimum value of $6.954 * 10^{-6}$. The range for m was less with maximum value of 1.14 and a minimum of 0.61 (Bryne, Gammisch and Thomas, 1980). The mean discharge rate, Q, can also be included in this equation over T, the length of the semi-diurnal tidal cycle of 44,700 sec:

$$A=a[T/2]m(Q)m \qquad \text{Eq. 2}$$

The numerical model was then parameterized with P based on water level data that was collected using a Conductivity-Temperature-Depth (CTD) gauge from 3/26/2013 to 1/17/ 2014 in the adjacent West Matagorda Bay (Huff and Feagin, 2017). The numerical model was iterated with variable P over the entire record. The maximum

spring tidal range was approximately 0.3 m; therefore, it is assumed this range will be fully realized within the internal body of water once the cross-section was excavated to a depth below the minimum water level that was recorded.

The water surface area was parameterized using a GIS dataset, derived from a visual classification of the water coverage in aerial imagery dating from 1958-2012 (Huff and Feagin, 2017). The surface area included all Old Town Lake and all connected waters down to the Fish Pass area (Figure 9). A 0.3 m water depth was assumed, based on both LIDAR elevation imagery and surveys taken using a Total Station. The Zimmerman Road surface area was excluded, as mentioned in Huff and Feagin (2017), but connectivity was uncertain due to a secondary barrier. The final surface area value multiplied by the maximum spring tidal range was assumed to be close to the available water volume for the maximum prism.

To compare the numerical model with true historical trends in the channel width, the observed channel throat width was regressed against the observed surface area of the impounded water basin, over the period from 1958 to 2012. This analysis was conducted using the imagery described above, whereby the width of the channel was measured at each time period by digitizing a transect in the GIS, at 1:1000 scale, at a location 128 m north of its connection with Old Town Lake (shown by small red line drawn in the channel in upper right inset portion of Figure 9). The channel was straight at this location, and approximately halfway between Old Town Lake and the debris pile. The measured lengths were then compared with the surface area for each period, and tested for strength of statistical correlation using standard linear regression.

Using the numerical model and regression analysis, the following scenario was subsequently modeled: a hydrologically idealized inlet cross-section based on a theoretical equilibrium with the maximum spring tide possible in this internal body of water.

Predicted Salinity after Removal

To identify the length of time necessary for salinity to equilibrate between the impounded water basin and the open bay, a STELLA model (v10, ISEE Systems) was developed. This parallel model used water level data collected in Old Town Lake and Matagorda Bay to parameterize one half of the model. Conductivity measurements from the CTD gauges were used to parameterize the second half of the model (in kg of salt). A volumetric ratio of kg of salt to water was created to get the value for parts per thousand. The difference in water level between Old Town Lake and the Bay acted as the driver for flow direction. If a higher water level existed in the Bay then it would flow into the marsh and vice versa. Salinity was treated as an independent factor. All water flowing from the Bay into Old Town Lake was at 30 ppt and the water flowing out of Old Town Lake was parameterized to be 45 ppt but was allowed to fluctuate depending on water inflow from the Bay.

The model assumed that the barrier was removed to a depth of 0.5 m, enabling the full 0.3 m tidal prism to exchange independent of the results from the aforementioned numerical model (water volume exchanges are independent of cross-section area if the depth axis is sufficient, though related through the water velocity).

Similar to the numerical model, the STELLA model was parameterized using the CTD-collected water level data from a gauge in adjacent West Matagorda Bay, baylevel, and the water level in the basin, basinlevel, increased with tidal inflow and decreased with tidal outflow at hourly time steps, t, based on the difference between the basin water level and the bay water level at a given point in time, where differ(t)=baylevel(t) – basinlevel(t).

Water was moved into or out of the impounded marsh when differ(t) was positive or negative respectively. Baylevel(t) acted as the driving variable; when water was higher in baylevel(t) than basinlevel(t), water moved into the marsh. The variable differ(t) was then converted to volume per hour, P(t) by multiplying by the impounded basin's surface area, where P(t)= differ(t)*basinarea. The STELLA model was thus iterated with variable volume per hour P(t), and assumed no barrier restricting flow.

P(t) determined the salinity values in the impounded basin. The quantity of salt exchanged in kg, salt, was derived from P(t) multiplied by the salinity of the exchanged water moving from the source basin to the sink basin, where salt=P(t)*salinity. The model assumed that water could not enter and exit the basin at the same time. Though more complex versions of the model included rainfall and evaporation components, they were excluded from the simulations as these phenomena introduced stochasticity and variation based on seasonal weather. Rather, the goal was to identify the average period of time required for the impounded basin salinity to equal the bay salinity, independent of the weather phenomena that would be experienced during barrier removal.

The model was initialized with bay salinities of 30 ppt and impounded basin salinities of 45 ppt. These values represented the mode of the observed CTD data for each location. The model was run 100 times. For every run, basinlevel started at the impounded basin's average water level according to the CTD data (0.46 m NAVD88). However, baylevel for each run was chosen to begin at a random start time in the CTD data record, and then follow the hourly CTD recorded water levels. This created unique infiltration and exfiltration rates for each run, as driven by the tides in the open bay, and was used to simulate the range of possible tidal cycle water levels that could exist for the exact date that the debris plug would be removed. For each iteration, the model was allowed to run for 1000 hours (though it was not computationally costly and ran quickly). Each iteration was manually started which took the majority of time and effort.

Barrier Dimension Measurement

A 3D model of the barrier was created using survey grade GPS measurements of the barrier. ArcMap 10.1 was used to interpolate the points using IDW. The 'Excavated Channel' was then subtracted from the surface model and the difference was used to estimate the volume removed.

Pre- and Post-Removal Verification of the Models

To verify both the tidal prism model and the STELLA salinity model, data was collected before and after barrier removal. Water velocity and flow direction, at multiple water depths, was measured for 10 days before and after the barrier removal (5/30/2015 to 6/9/2015 for pre-removal sampling and 7/30/2015 to 8/10/2015 for post-removal

sampling). Samples were collected at a frequency of 1 sample every 30 minutes. Each sample was taken at 1 Hz over a duration of 60 seconds and the average of those values was recorded. A bin width of 1 cm was used for the entire water column starting 7 cm from the Aquadopp head and ending at the water's surface. This was done using a Nortek Aquadopp acoustic doppler profiler placed at the bottom of the channel on the impounded side of the barrier, yielding water velocities in m/sec for every cm of water depth excluding a 7cm blanking distance from the sensor head. The Aquadopp was physically strapped to a PVC pipe frame that had legs that were sunk to a depth of 30cm into the channel floor. The sensor was placed at the deepest point in the center of the channel with the sensor oriented in line with the channel direction. To guarantee that the surface of the water could be seen with an upward looking acoustic sensor, a CTD tidal gauge was paired with the profiler. This coupled placement allowed for post-hoc clipping of the Aquadopp values to each time-specific water level.

Results

Recorded sensor data was used to verify the modeled components. Each model was treated as separate from the others, and outputs from one model were not used to parameterize the next model. This was done to reduce compounded error, and allow for independent model products. This further allowed for testing of independent model agreement.

Numerical Model for the Ideal Cross-Section of Removal

The idealized cross-section is in theoretical equilibrium with its tidal prism (as defined by the empirical coefficients in Eq. 1 and 2, sourced from the various literature

sources mentioned), and thus the required cross-section increased from 1958 to 2012 (Figure 11). During this time period, the size of the maximum spring tidal prism increased from 194,015 m^3 to 282,603 m^3, because of the conversion of marsh to open water. The cross-sectional channel area increased regardless of the exact value used for *a* and *m*, as varied by citation. The resulting cross section produced a range from 12 to 25 m^2.

Results from the empirical GIS analysis of aerial photography from 1958 to 2012 corroborated this numerical relationship in concept (Figure 12a-b); the observed channel width increased (from 10 m to 21 m, a 210% increase) at approximately the same rate as the observed water surface area in the marsh complex (from 647,018 m^2 to 942,011 m^2, a 145% increase). The channel width was linearly and positively related to water surface area ($y=2.8564x-7.0582$, $r^2=0.775936$).

A minimal impact cross section was selected at approximately 13.5m^2, where all the shell and mud debris were removed from the 'Excavated Channel' so that the inlet was within the range of an ideal equilibrium with its tidal prism (orange dot in Figure 11). The modeled water velocity ranged, in the inlet during a maximum spring tide event, between 0.51 and 1.11 m/sec when using the variations of Eq. 1 by citation for an ideal cross-sectional area. The 'Excavated Channel' fell within this range at 0.94 m/sec (Figure 13). For the large majority of the tidal cycle, the predicted velocity was much lower for the 'Excavated Channel', however, with the 50th percentile at 0.38 m/sec (Figure 14).

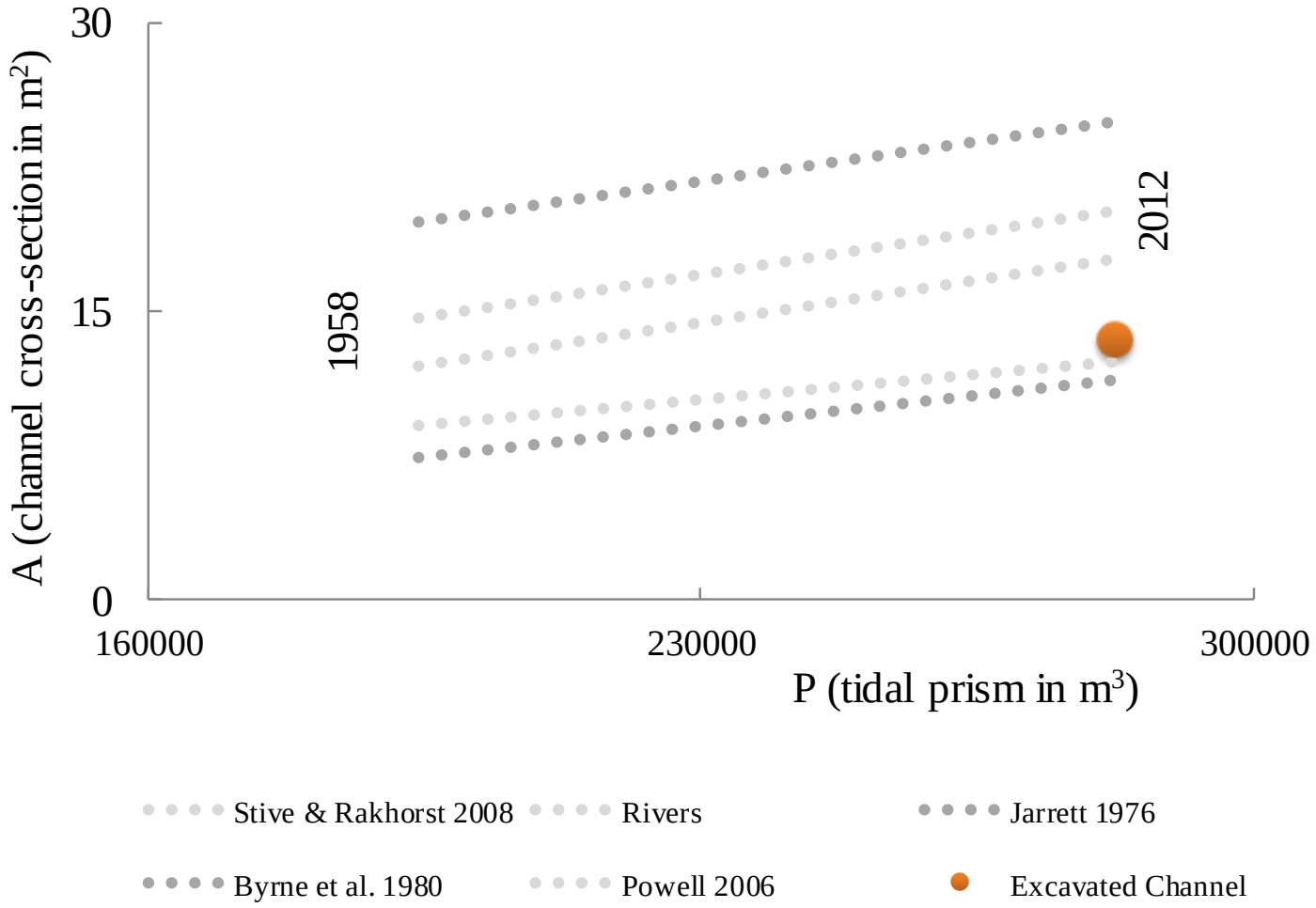

Figure 11: The 'Excavated Channel' scenario fits within the bounds of theoretical equilibrium for the Magnolia Inlet. Theoretical cross-sections assume varying water volume from 1958-2012 for the wetlands area (depicted by lines); the two options (orange circles) assume 2012 water volume only.

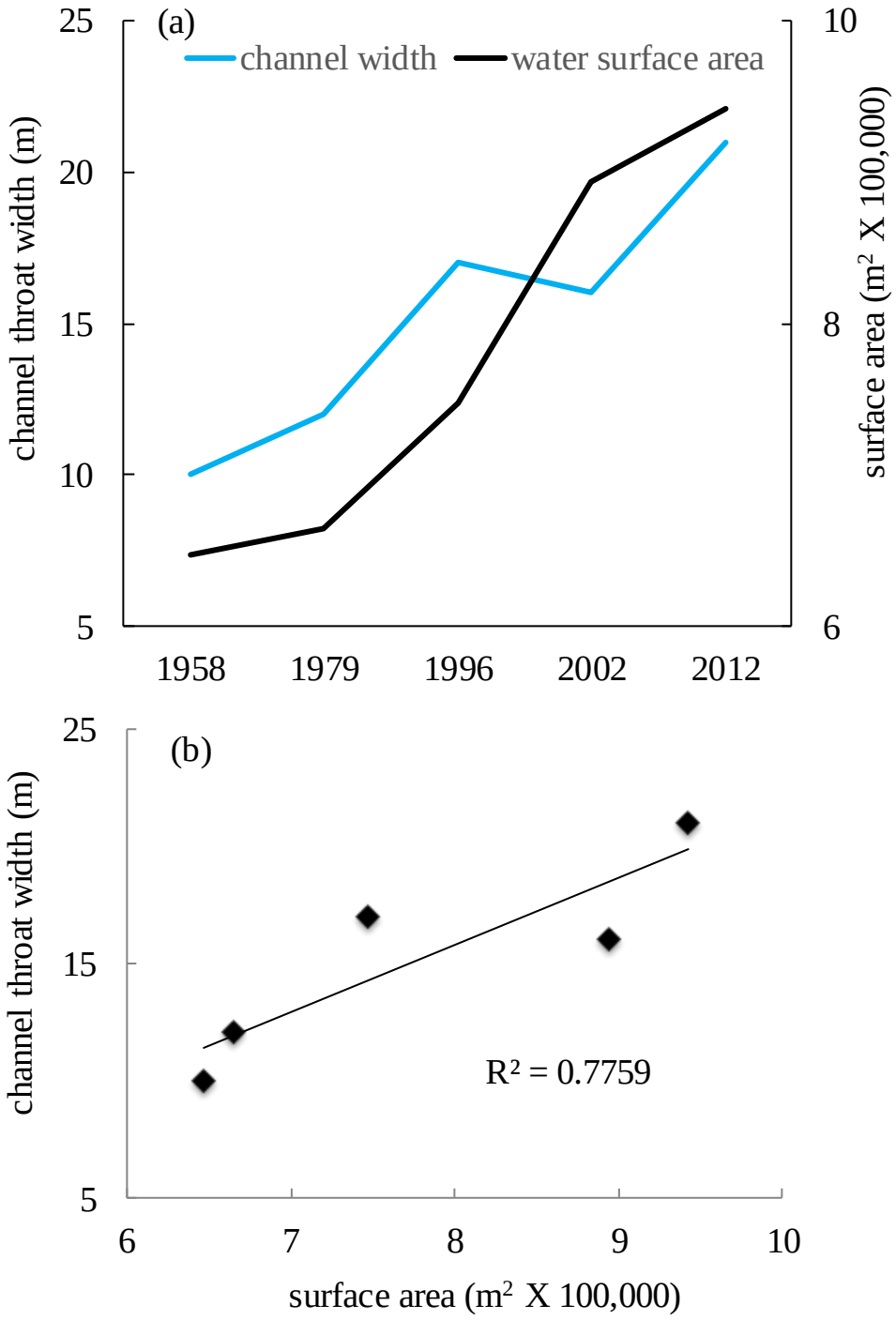

Figure 12: Channel throat width and water surface area change, over time (a), and plotted against each other (b).

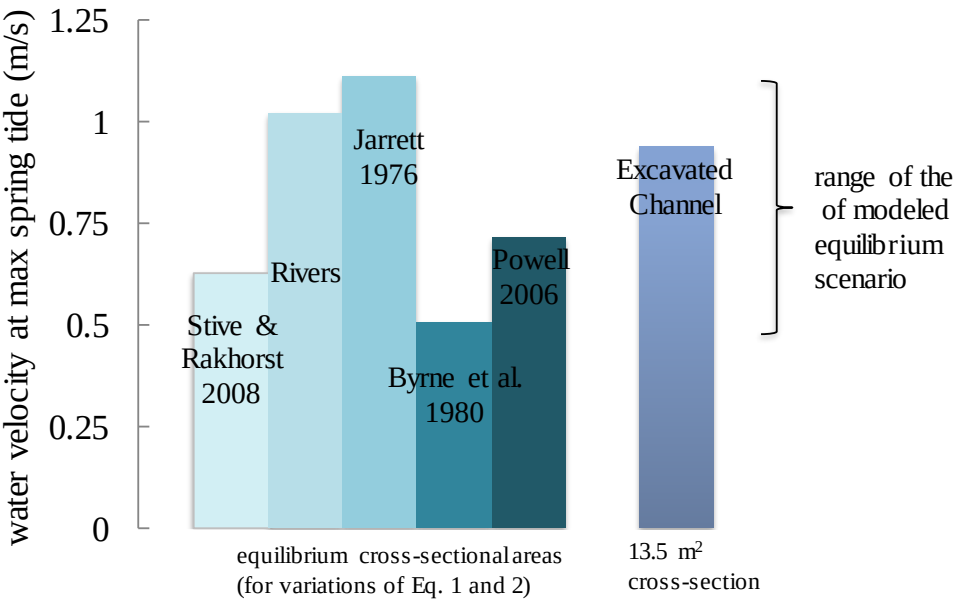

Figure 13: Predicted water velocity at maximum spring tide for the 'Excavated Channel' scenario versus an inlet at theoretical equilibrium with the prism.

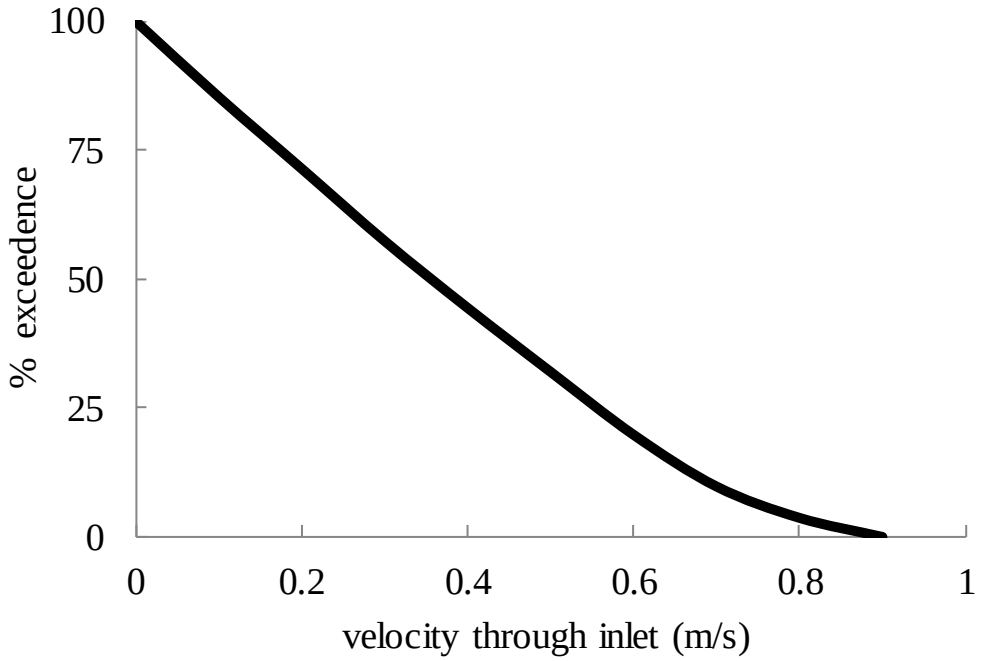

Figure 14: Percent of the time that water velocity will exceed a given value, after excavating the 'Excavated Channel' cut option.

The acoustic profiler data showed an average water velocity of 0.029 m/sec before removal and 0.13 m/sec after (Figure 13). After barrier removal, the maximum tidal cycle change was 3.45 cm (wl-change) in 8 hours (time-change). This fluctuation equated to an average velocity in the inlet channel of 0.112 m/sec. The numerical model estimated a tidal fluctuation of 5 cm in 12 hours, resulting in an approximately 0.15 m/sec water velocity. A ratio was created to directly compare the values. Centimeter values were converted to m and all hour values were converted to seconds ((wl-change*0.01)/(time-change*120)/wt-velocity). The ratio resulted in change in water level in m/s over water velocity in m/s. The Aquadopp measurements produced 0.032 with the numerical model producing a value of 0.030. Thus, the model generally reflected the conditions seen within the marsh after removal of the hydrologic barrier.

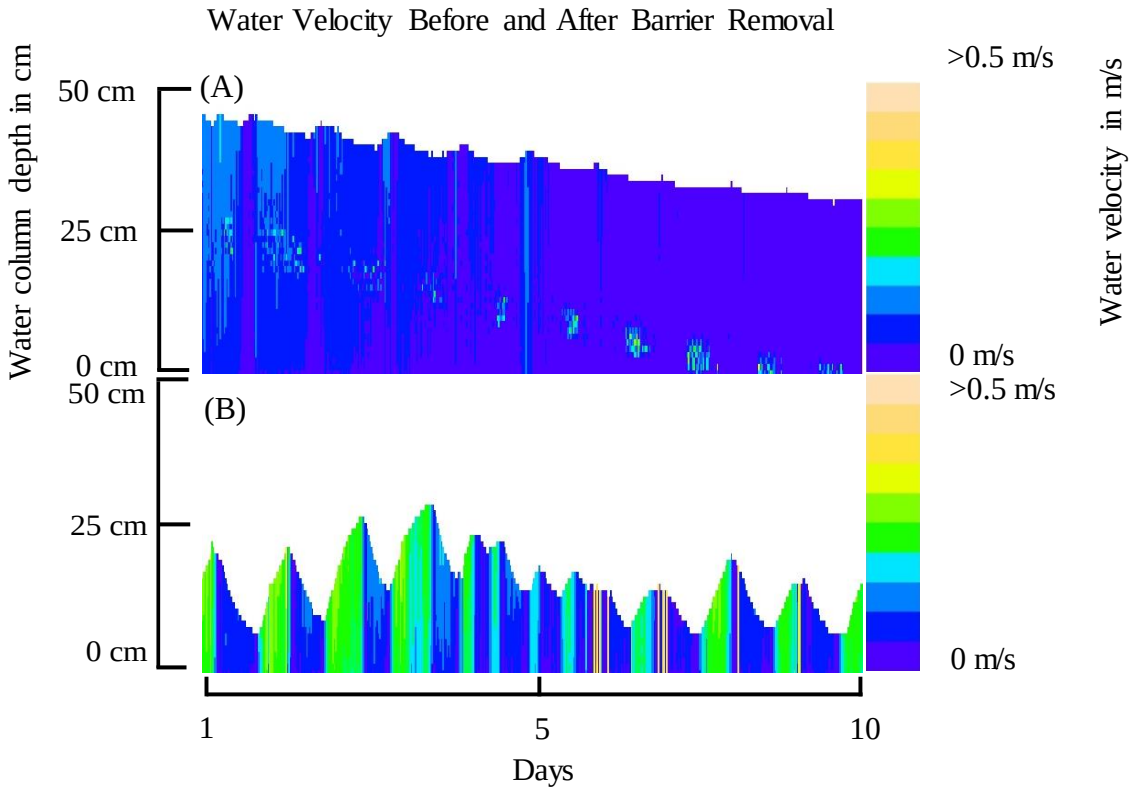

Figure 15: Water velocity comparison of entire water column before and after barrier removal. The collection time was at separate dates but for 10 days each time (5/30/2015 to 6/9/2015 for pre-removal sampling and 7/30/2015 to 8/10/2015 for post-removal sampling).

The water level pre-removal (Figure 13a), was considerably higher versus post-removal (Figure 13b). This was due to the influence of the hydrologic barrier on tide fluctuations. During the first time frame only the highest tides could influence the measured water level. When the tides retreated into the open bay, the water level within the marsh was only able to decrease to the level of the top of the barrier. Consequently, only the very highest portion of the tidal cycle was observable in the data. However, in the post removal data, the barrier no longer influences the water level and the entire tidal

cycle was observed in the marsh. This situation, in conjunction with the relatively low water levels during the summer, produced the difference in water level that can be seen in Figure 14, though both the velocities and the pattern of up and down tidal cycling indicates greater connection to Matagorda Bay. A linear regression analysis was performed on the water level data, splitting it into two different groups. The first group was pre-barrier removal, and the second was after barrier removal. This analysis was performed for North Old Town Lake (NOTL) against Matagorda Bay, and for South Zimmerman Road and North Zimmerman Road. It was found that before the removal NOTL and the bay had an r^2 of 0.9179 and after removal the value rose to $r^2 = 0.9816$. For the Zimmerman Road comparison the r^2 values barely change ($r^2 = 0.9998$ pre-removal, and $r^2 = 0.9972$ post removal). All p values for the 4 regressions were (p-value < 0.0001).

Predicted Salinity after Removal

The STELLA-modeled impounded basin reached 30 ppt (46.9 mS) (same as the open bay, a decrease of 15 ppt (23.4 mS) from the initialized value, Figure 15) within an average of 10.30 days ± 1.75 days (247.3 hours ± 42 hours). Across 100 runs of the model, the maximum time frame was 12.83 days (307.9 hours) and the minimum was 6 days (144 hours).

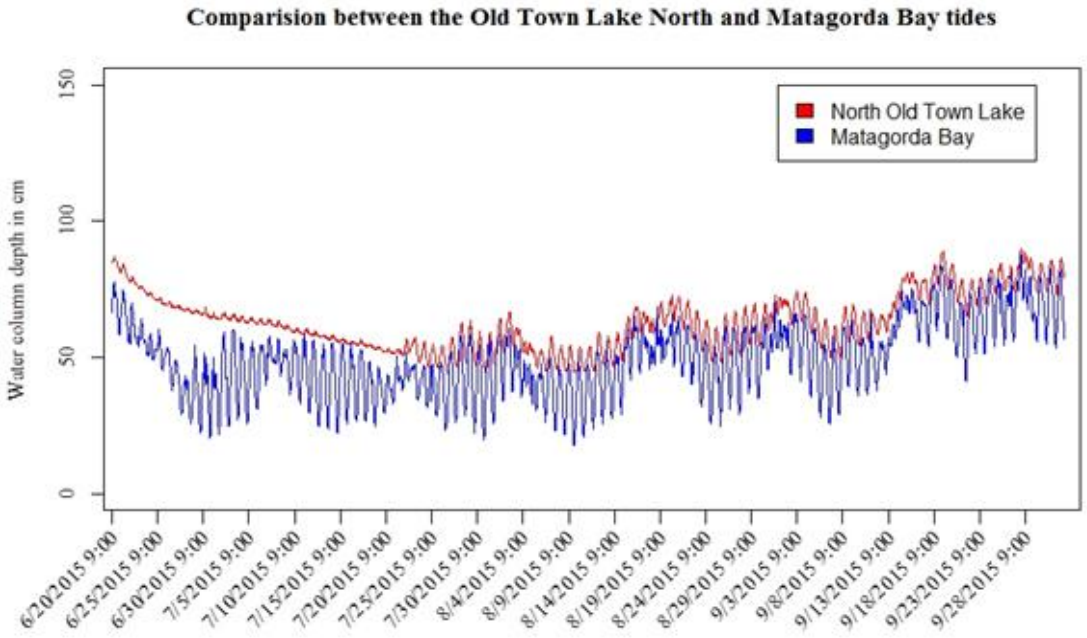

Figure 16: Water levels listed in centimeters for the north end of Old Town Lake (red) and the Matagorda Bay (blue).

Post-removal, field-verified time for salinity to reach equilibrium was approximately 2.96 days. The salinity difference between the marsh and the bay at the time of removal was only 2.45 ppt. The rate of change of 0.83 ppt/day was under the predicted rate ranging from 1.17 ppt/day to 2.50 ppt/day in the STELLA salinity model (Figure 15).

Debris Quantities

GPS based survey work produced a three-dimensional model of the debris pile (Figure 16). Based on a 0.5 m excavation depth and the three-dimensional model of the debris pile, the total volume of the debris for removal (composed of mud and oyster shell) was

estimated at 779.37 m^3. This equated to approximately 100 small dump truck loads of material and 3 days of excavation work).

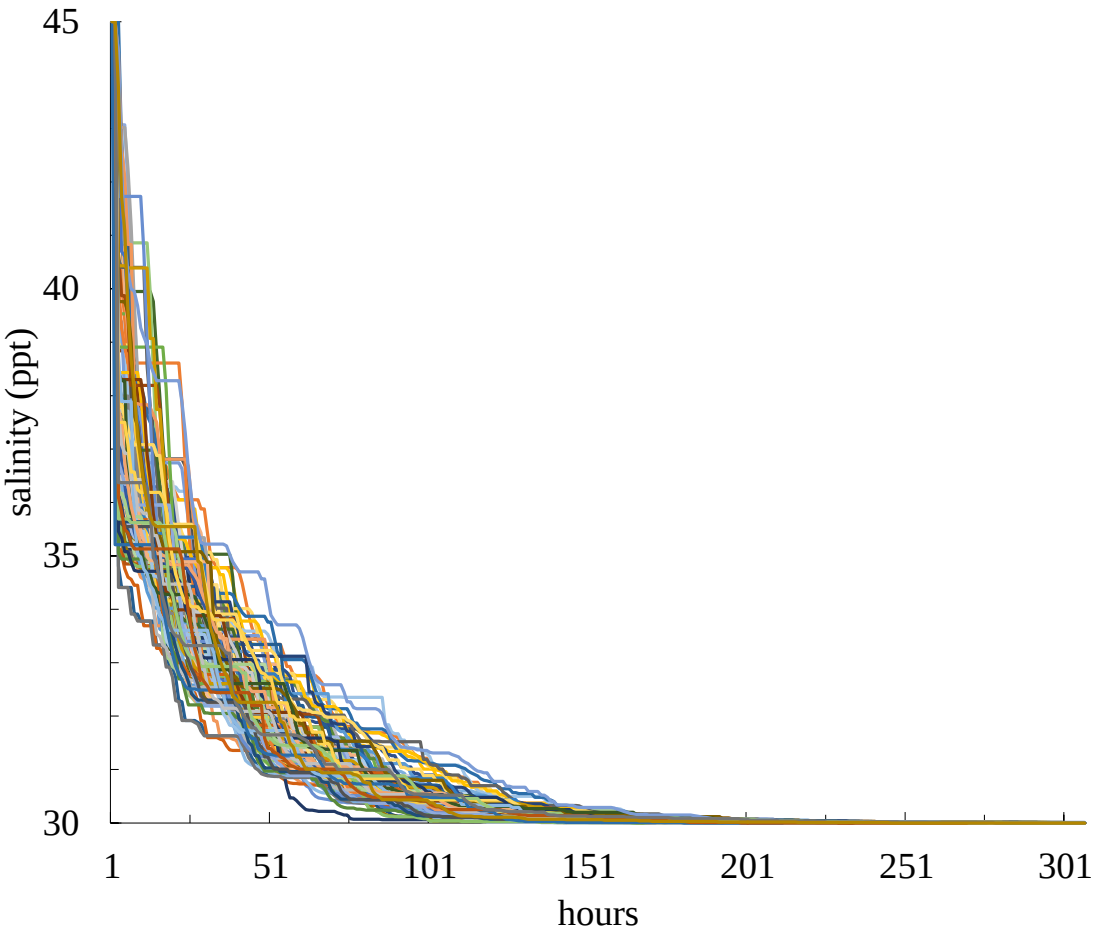

Figure 17: Length of time until salinity equilibrates between the marsh basin and the open bay, as derived by the STELLA salinity model performed 100 times.

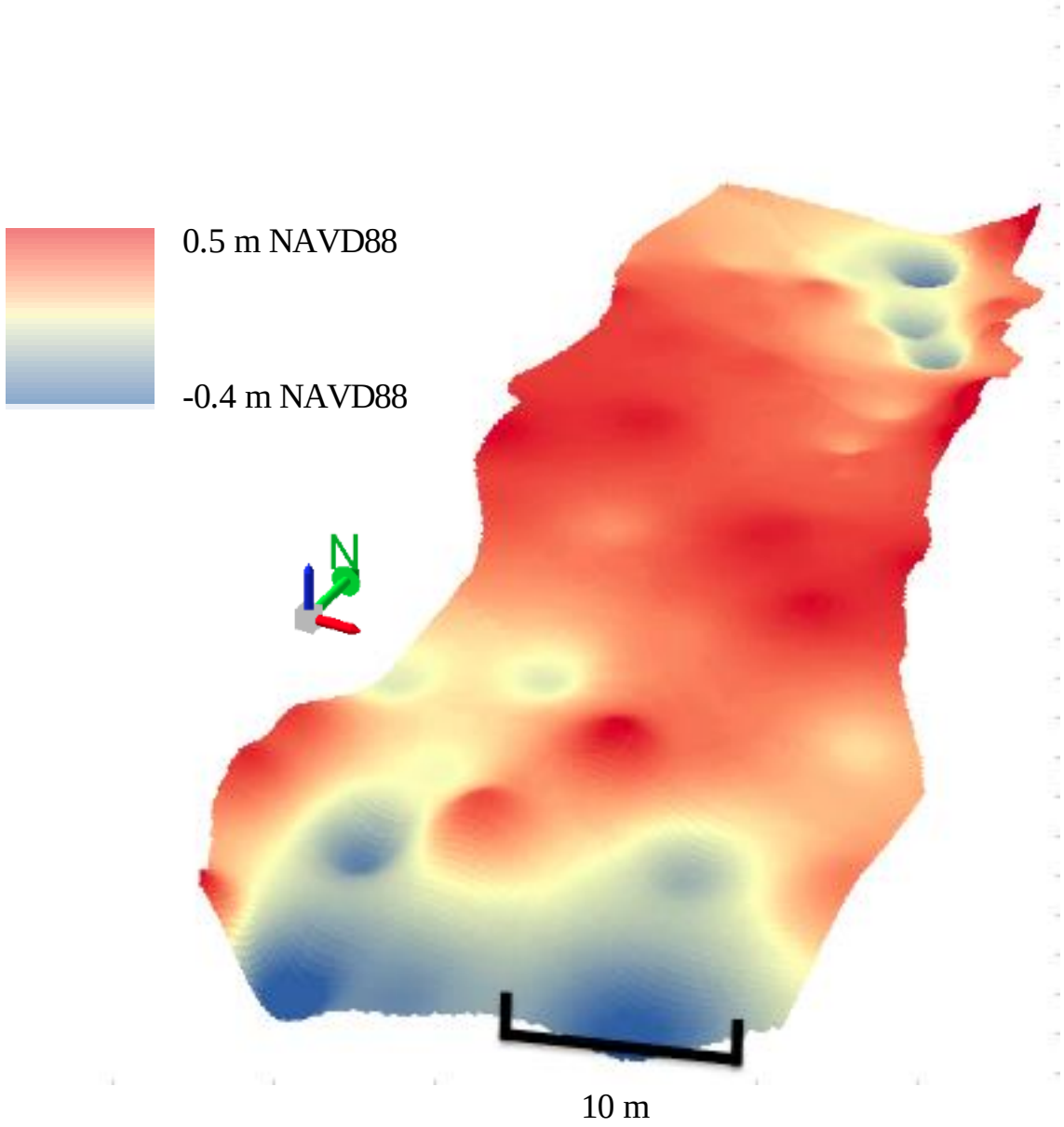

Figure 18: Three-dimensional model of the debris pile. Viewed from the south of the debris plug looking to the north along the stream channel. Blue color locations generally coincide with water, reds with the debris pile.

Discussion

Based on the modeling, a cross-sectional area of 13.5 m^2 was determined to be the ideal goal for the excavation of the debris plug in the channel at Matagorda Inlet. The excavation was started on June 21, 2015 and completed on June 23, 2015. The water flow velocities were within acceptable ranges such that scouring did not become a major problem (Jarret, 1976). Conversely, it was predicted that the velocities would remain high enough during maximum spring tidal flows (approximately 0.8 m/sec average) to promote sediment transport and reduce the probability that the channel will revert to a blocked state. Sediment transport speeds occur around 0.6 m/sec for fine sand particles (a major constituent of the debris with a mean of 63 microns in diameter (4 Φ)) (Jarret, 1976). Extensive sediment transport models were not conducted as the inlet is periodically dredged closer to the inlets connection with the bay. The main concern was removing the shell debris as this was too large to be eroded or suspended under normal tidal flow.

The numerical model was confirmed with the acoustic profiler data to show that realized velocities were near the predicted velocities (0.9 m/s). This supports the conclusion that the velocities will be sufficient to mitigate the chances of sedimentation occurring and blocking the channel in the future (Powell et al., 2006). With spring tidal velocities being sufficient to keep the channel open, the hydrologic equalization between the marsh and the bay will likely remain in a state of dynamic equilibrium.

The STELLA model results also showed that the long-term outcome of the hydrologic restoration is good. Even though the model predicted a longer time frame to

reach salinity equilibrium, a shorter time frame (as seen in the data) to equalization is desirable. The model predicted a salinity difference of 15 ppt at the time of reconnection, whereas the difference was only 2.45 ppt during the time of reconnection. Therefore, a significantly shorter time for equalization can be expected as salinities fluctuate in Matagorda Bay or in the marsh. With the estimated and verified rates of change, the data shows that the model predictions were indicative of healthy marsh conditions.

With the abiotic conditions of water flow and salinity in equilibrium, the biotic community now can recover. Fluctuating tidal conditions are now suitable for the spatial expansion of marsh grasses to colonize previously continuously flooded areas. This allows for the growth of nursery habitat and increases escape cover for developing nekton (Adams and Bate, 1995). With the increase in number of small "bait" fish, an increase in the number of larger "sport" fish is expected. Anecdotally, this has been the case thus far, and based on communications with the fishing industry in the local community the western Matagorda Bay area has been stimulated.

Conclusion

The prognosis for this marsh complex is good. With the barrier removed, the tides are once again the driving factor in regulating water salinity. The channel cross section is in equilibrium with the historical evidence, allowing for a stable channel. With a stable hydrologic connection, the vegetative communities are now able to colonize previously inhospitable areas, and allow nekton consistent access across the marsh and the bay.

CHAPTER IV

IMPROVING TIDAL PREDICTIONS WITH INTEGRATION OF WIND DATA IN THE GULF OF MEXICO

Introduction and Literature Review

Historically, tide estimation was built on knowledge of lunar and solar cycles to give the timing and cycling of the tides. These models combine the gravitational pull placed on the earth by the moon, sun, and the centrifugal forces (NOAA, 1998; Matsumoto, Takanezawa, and Ooe, 2000). Tides have been measured and recorded since the early 1800 in the United States, and today tide measurements and predictions are crucial for navigating coastal waterways (NOAA, 2016). The National Oceanic and Atmospheric Administration (NOAA) provides a user-friendly and internet-accessible product that incorporates empirical data with astronomical cycles to make tide predictions. However, empirical tuning of the NOAA model takes approximately 18.6 years, which is the length of the astronomical cycle influencing tides (NOAA, 2013). These predictions are accurate at capturing the major physical forces that influence tides (Mukai et al., 2001). Predictions can be made years in advance as astronomical tide factors are highly regular (NASA, ND; NOAA, 2013). However, several additional factors, such as Ekman transport, wind direction, wind speed, storms, system location (bay or open water), bay inlet dimensions and subsurface bathymetry, are known to affect the observed water level and these factors generally are not included in NOAA tide models (NOAA, 2008; NASA, ND; Cheng and Smith, 1998). In shallow water and

micro-tidal coastlines, these factors have great influence on the overall tide level (NOAA, 2008).

In a micro-tidal basin such as the Gulf of Mexico, it is not unusual to see the observed water levels exceed or fall below the NOAA estimates by a factor of two greater than the maximum astronomical effect (Lefevre, Le Provost, and Lyard, 2000; Zavala-Hidalgo, Morey, and O'Brien, 2003). A swing between an accurate prediction and an inaccurate prediction of this magnitude can happen in only a few hours, and in some cases, have left ships stranded in shallow water until favorable tides occurred for their extrication (Coast Guard News, 2015; NOAA, 2001; NOAA, 2016). Failing to correctly estimate both high tide (unexpected inundation events) and low tide conditions (unexpected problems with draft passage) can be equally detrimental. Moreover, as relative sea level rise continues, the margin between a safe water level and flooding becomes narrower (NOAA, 2001), and the importance of an accurate prediction becomes greater. In summary, the difference between the NOAA predicted and observable water level poses a great problem for the utilization, recreation, and navigation of shallow basins.

Traditionally, numerical models have been created to address these problems (Zavala-Hidalgo, Morey, and O'Brien, 2003) but they are often limited to local application. Alternately, coarse scale tidal models can focus on oceanic circulation (Padman et al., 2002), however these models lose their effectiveness closer to shore (Matsurmoto, Takanezawa and Ooe, 2000). There is a lack of universal method to

address the ‘wind-tide’ problem in bays and shallow water coasts, where much navigation is conducted.

To improve NOAA tide level predictions in this manner, we incorporated wind effects on water level into an Enhanced Tide Model (ETM). This model adjusts the NOAA water level predictions, using wind data sets acquired from the US National Weather Service (NWS).

Methods

The ETM was broken into two separate modeling procedures. The first being the base model, which formed the framework for the second half of the model, the predictive model. The base model takes historical tide data, along with historical wind speed and wind direction, analyses it, and creates a matrix. The Predictive Model then uses this matrix in combination with future predicted wind speed and direction data to create the tidal predictions. These predictions are then graphed and linked to a map.

Base Model

The base model follows an empirical approach based on trends in historical data sets, namely NOAA wind speed, NOAA wind direction, NOAA predicted water level, and NOAA observed water level. These data sets were downloaded from NOAA (Tides and Currents, 2017) websites, and saved in .csv files by the month the data was collected. This procedure resulted in approximately 6,000 months of data gathered from 89 different NOAA gauges across the Gulf of Mexico and the East coast of Florida. Any data available for each gauge from 2010 to 2015 was collected using R programming web applications to extract the data and save the files into a database (R Core Team,

2017). Date formats were corrected and the data was matched for each time frame. If one of the four data sets (NOAA wind speed, NOAA wind direction, NOAA predicted water level, NOAA observed water level) was absent for a given time frame, then that entire time frame was deleted from the compiled database. This procedure resulted in only complete records being kept and used in the model.

R programming was used for every aspect of the model (R Core Team, 2017). Python was briefly considered for portions of the web data extraction, but R proved to be appropriate for XML based web data gathering. R also has very powerful data visualization tools and thus it was decided to use R for the complete project.

Once the data was gathered, a unique prediction matrix was created for each individual NOAA tidal station with wind speed on the x axis and wind direction on the y axis. The matrix contained 30 columns and 360 rows. Wind speeds above 50 miles per hour (mph) were not included in the model, as there was insufficient data for these types of events to be consistently considered, but moreover other processes such as regional scale storm surge begin to predominate at these speeds, thus limiting predictability. The difference (diff) between the NOAA predicted water level at the station (pred) and NOAA's observed water level (obs) was taken for each hour (pred - obs = diff). Each occurrence of the same wind speed (ws) and wind direction (wd) for the selected station was listed, and the median diff value was entered in the matrix for that (ws) and (wd) combination.

Even with approximately five years of data for each station, a few cells were left empty in each matrix, and thus interpolation was used to fill these missing values (the R

"interp" function from the R package "akima") (Akima and Gebhardt, 2016). The interpolation method was tested against several data filling methods such as a moving window, spline interpolation, linear regression, kriging, and IDW. Each method was evaluated independently and the computationally efficient and reasonable method was used. If the interpolation program was unable to fill a gap in data, the missing value was left empty and averaging was used in the next step (the predictive model) to adjust for these gaps.

Predictive Model

To make hourly predictions for water level at each station for up to 72 hours ahead of time, US National Weather Service (NWS) point forecasts of wind direction (wd) and wind speed (ws) were obtained (NWS, 2017). NOAA tide station water level predictions were also obtained, though importantly they were only based on astronomical considerations. The (diff) value in the selected cell from the base model was added to NOAA's future predicted tide level (pred) to adjust for wind influence and create the predicted tide level (ETM-pred), thus (diff) + (pred) = (ETM-pred). Importantly in the NWS point forecast dataset, exact wind direction in terms of angular degrees were not given, but rather a general direction of N, NNE, E, SSE, S, SSW, W, NNW. As an example, E corresponds to the values within 68 to 112 degrees. The mean of the diff values in the rows (which correspond to wind direction) for 68 to 112 degrees took the place of the diff value that was used in combination with pred to achieve the ETM-pred value.

The ETM-pred value was then cleaned of data spikes using the smooth.spline function ("stats" package) in R with the val parameter set at 1 (a less aggressive level of smoothing that still only removed the largest spikes) and with a weighting nknots factor of (prediction length in hours/val) (R Core Team, 2017). The nknots act as "node" locations for the connection of separate portions of the arc spline arc and acting as a control point.

Finally, the ETM-pred value was further tuned by incorporating real time observations from the NOAA station information. If ETM-pred was not equivalent to obs, then the difference between ETM-pred and obs was calculated and all subsequent ETM-pred predictions were shifted accordingly. The influence of the adjustment linearly decayed over each hour h out to 48 hours total (the decay rate was 1/48 of the difference between ETM-pred and obs per hour) based on an assumption of temporal autocorrelation, where predictions now are more likely to be similar to subsequent predictions close in time, as compared to those happening more distant in time. For hours 48 to 72 of ETM-pred, no further tuning was made. From here forward, we refer to final predictive output as sourcing from the ETM model, which is in effect a combination of the base model and the predictive model.

Model Testing and Validation

We conducted three types of tests to assess the validity of the ETM model. For the first, the ETM was fed all the historic data for ws, wd and NOAA's predicted tide levels, for all stations in the Gulf of Mexico. In this test, we were forced to utilize NOAA's actual observed ws and wd recorded at each station in the past, because NWS

point forecasts from past dates are not publicly-available. Thus, this test of validation uses verified wind data, and can only assess the ability of perfect knowledge on wind to accurately predict the observed water level. This test essentially validates the base model alone. For each station, the predicted values of ETM were then compared to NOAA's observed water level and the average deviation was recorded. For comparison, NOAA's own predicted values were compared with the NOAA observed water level and the average deviation recorded. Next, the average deviation of the ETM and the NOAA predictions were compared to obtain the percent improvement of the ETM over-and-above NOAA's predictions (((NOAA prediction/ ETM prediction)-1)*100). We then mapped the distribution of the improvements over the NOAA predictions, using ArcMap 10.2.2 (NOAA, 2008).

For the second analysis, NOAA's predicted tide levels were used in similar fashion as input, but ws and wd were sourced from NWS, present-day, real time data sets, and subsequently the ETM prediction was saved. Thus, this test assesses the predictive portion of the model, but any error could be both due to ETM-based errors, or errors in NWS-predictions in real time. This test essentially validates the predictive model, and includes the three-hour adjustment factor as described in the previous section. However, like the first test, the predicted values of ETM were then compared to NOAA's observed water level and the average deviation was recorded, as well as the deviation between NOAA's predicted and observed water level, and the deviations were compared.

For the third analysis, NWS wind speed (ws) predictions were subtracted by NOAA observed wind speed to get the difference between observed wind speed and predicted wind speed. This was important to understand the error in the wind predictions as the ETM is based on those wind predictions. Then, the difference between the ETM tide predictions and the NOAA observed water level was taken for the same time frame as the above wind measurements. The two data sets were then regressed against each other. The accuracy of NWS wind direction (wd) prediction was not assessed.

Results

Base Model

For the first test, the ability of the base model to improve tidal water level prediction was dependent on location (Figure 19). In open water the model performed very well as seen on the western coast of Florida. Bays proved to be more difficult to predict as a myriad of factors such as inlet dimensions and changes in bathymetry can cause historic data drift and result in less predictive accuracy for the model. However, the areas with the least accuracy were riverine areas. This was due to the model being unable to contend with the stochastic events of freshwater input. While these areas are still tidal, the model's inclusion of wind data does not directly relate to water level changes related to river flow volumes, as they are distinct physical elements. One of the future goals will be to filter these locations or integrate river flow volume predictions. ETM accuracy and number of hours of training data per gauge was examined and there was a weakly significant trend ($r^2 = 0.0491$, $y = 1E\text{-}04x + 8.1842$, p value = 0.09; Figure

20). A total of 18.6 years was needed for NOAA's model, and thus it would be good to see if a longer and larger data set produced trends that are currently undetectable.

For the second test, the ETM predicted water level showed a mean difference from NOAA observed water level across all gauges of 14.08% from the value of the observed water level (when this value was averaged over 36 hours from the last ETM model prediction), as compared to NOAA's predicted values which had a mean difference from NOAA observed water level of 20.17%. The ETM showed a 6.09% improvement in accuracy over NOAA predictions from 0-36 hours from the last ETM prediction across all NOAA gauges in the Gulf of Mexico. At the 60 hour mark after the prediction was made, the ETM's predictive mean deviation from observed water level (calculated the same as above) was 16.49% with NOAA' predictive mean deviation at 19.51%. At 72 hours, the ETM predictive mean error was at 15.49% with the NOAA model predictive mean error at 19.03%. Thus, the ETM showed a 3.54% mean increase in accuracy over NOAA predicted water level at 72 hours out from the last EMT prediction.

For the third test, there was no clear trend between predicted wind error and ETM model error ($p=0.6066$ $r^2=0.008125$) (Figure 21).

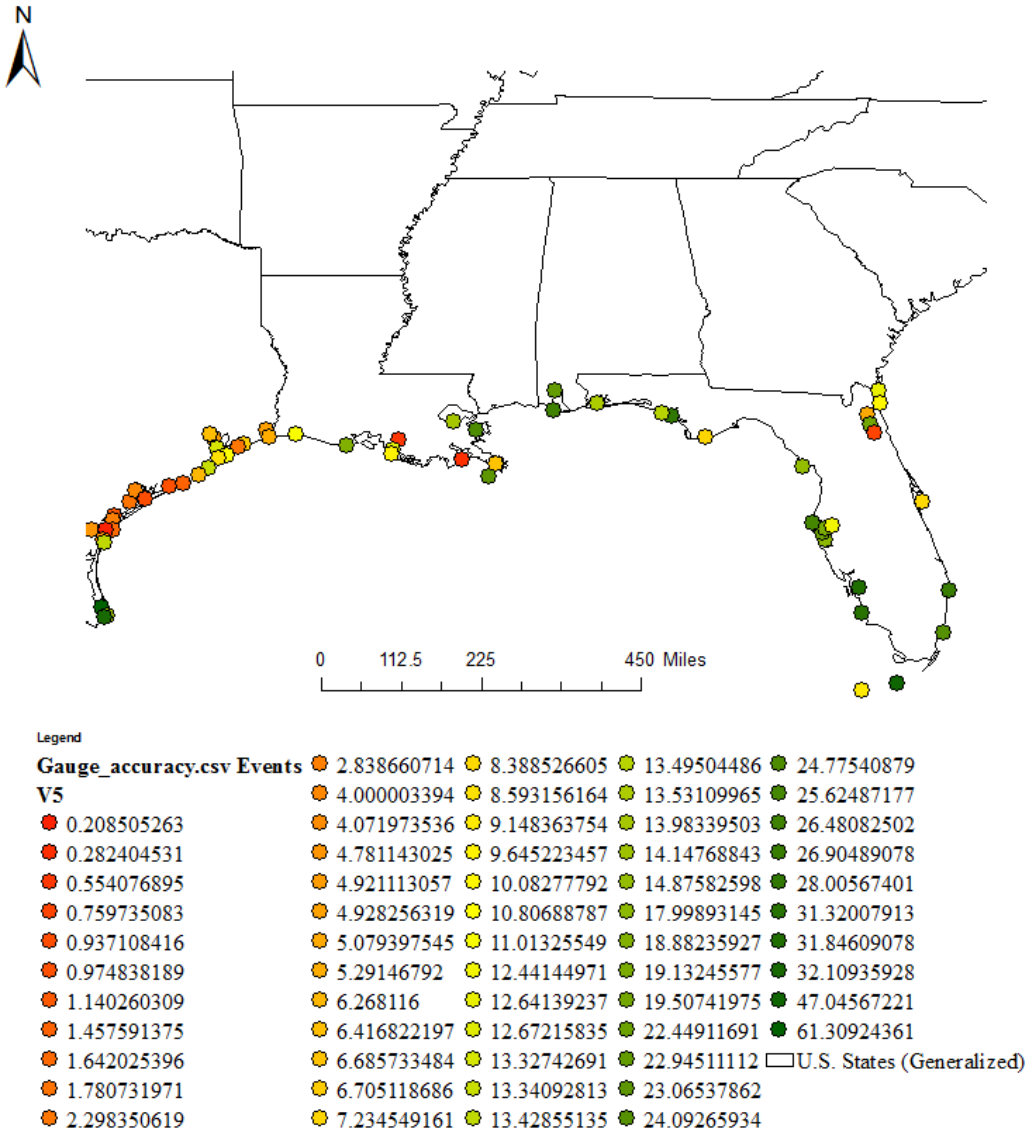

Figure 19: Map of station locations using the Gulf of Mexico as an example. This map also details model accuracy with the legend showing the ETM tide prediction percent improvement over NOAA predicted tide levels. Red indicates lower accuracy (0.21% increase in ETM prediction accuracy over NOAA predictions) while green indicates high accuracy (61.31% increase in ETM prediction accuracy over NOAA predictions). Even the lowest accuracy is still an improvement over NOAA tide estimates.

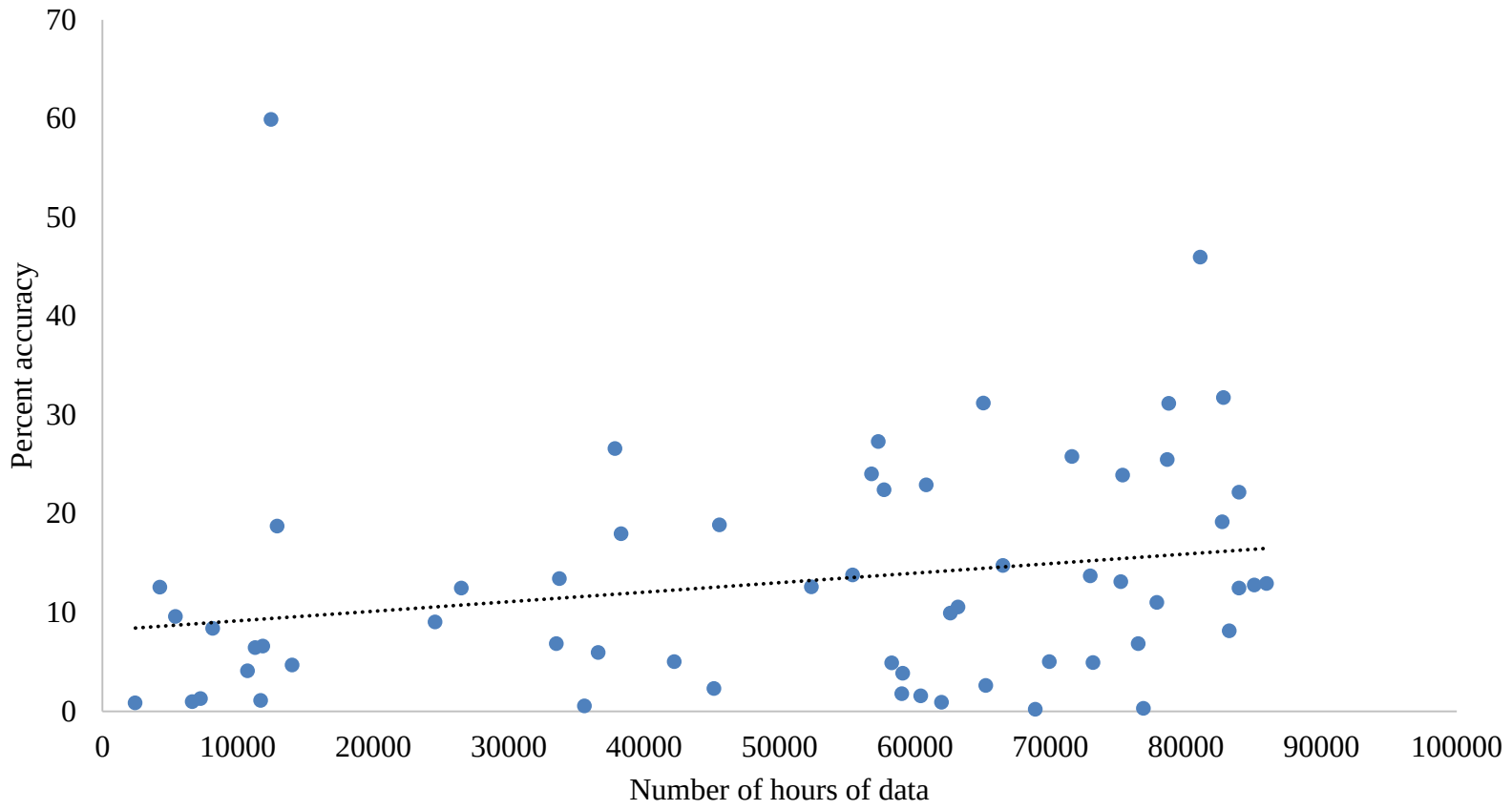

Figure 20: ETM percent predictive accuracy improvement over NOAA. The percent accuracy improvement is regressed against the number of hours of historic data that was used to create the predictive matrix in the base model.

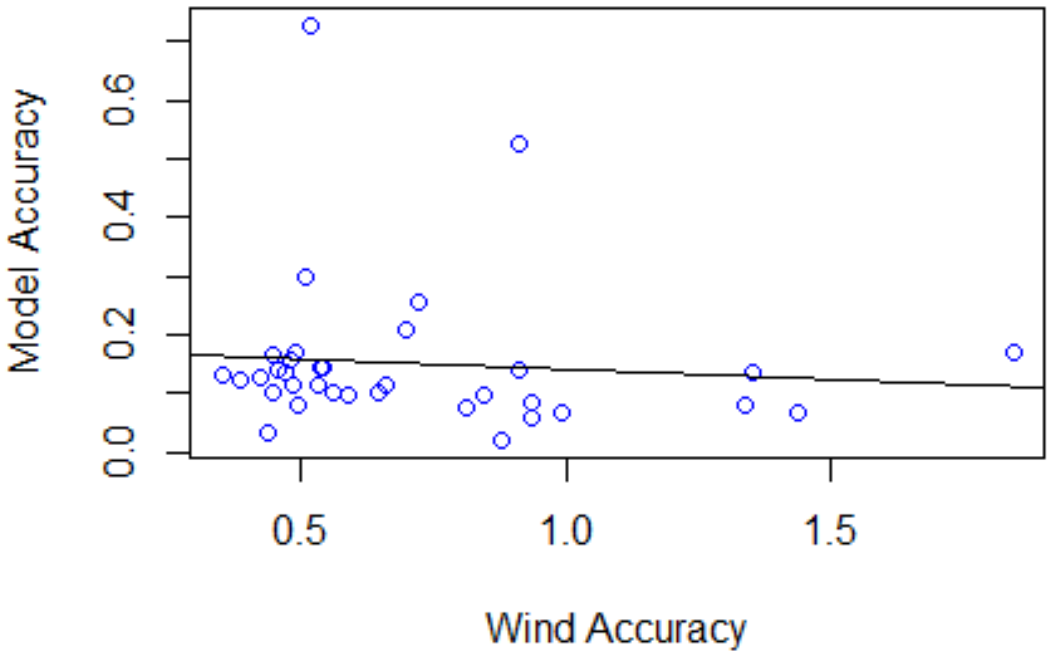

Figure 21: Linear regression between (the difference between NWS predicted wind speed and NOAA recorded wind speed) listed on the x axis and (the difference between ETM predicted water level and NOAA observed water level) on the y axis.

Discussion

Run Time Considerations

The data-gathering portion of the base model is relatively costly in computing time and requires approximately three to five days to gather and calculate all the data for the 89 NOAA gauges across the Gulf of Mexico. Fortunately, this procedure only needs to be run once, or updated as more historical data becomes available and is deemed important to include into the base model. While there is not a strong correlation between number of hours of data collected and the accuracy of the model predictions, the trend is nevertheless positive. Thus, another further development of the base model could also include greater data-gathering extending back greater than 20 years.

For the real-time ETM predictive model, the computational time was substantially lower and runs on an aged AMD dual core laptop in 15 minutes, and a more modern eight core machine in six minutes. These rates could likely be improved with some code optimization and moving away from "for-loop" structures to "apply" structures in R programming since the typical use of the ETM by the programmer is produce predictive models, this speed is sufficient to provide real-time data to outside users.

According to our testing, the most computationally costly procedure is interpolation of the matrix and kriging was the costliest version that we tested. The time frame for this model to run was approximately 90 days. It was also found that the different interpolation methods highly influenced the overall accuracy of the model. One area of potential improvement is the use of different interpolation methods in

creation of the matrix such as linear regression, kriging, IDW, and moving window analysis. The linear regression interpolation showed a 74% reduction in accuracy over NOAA's astronomical prediction. A column wise moving window averaging model was used to try and fill data gaps and resulted in 94% reduction in accuracy. A kriging analysis was started to fill the matrix but this method was not easily scalable and was very difficult to use. The analysis was unable to complete due to data compatibility errors. This method for data interpolation was subsequently abandoned. The same occurred for IDW. The R interpolation method (interp) was much faster and much more stable than other methods and produced an increase in accuracy anywhere between 0.21% and 61.31%. Another potential way to improve or speed up the interpolation is to use linear regression, however this procedure substantially-decreased accuracy (53.78% decrease in accuracy). The interpolation method highly influenced the accuracy of the model and this is likely due to the matrix structure of the data. While unconfirmed, it is likely that the data displays a high degree of autocorrelation and thus needs a method that does not treat individual columns or rows as discrete data sets.

Future Work and Potential Improvements to ETM

One of the short-comings of the ETM is that by design it is based on weather forecasts. If the wind predictions are wrong the model will be wrong. Thus, this fundamental source of error must to be accepted in the model to make predictions. This is to be expected as the weather data becomes more unreliable the further out in time. However, there appears to be a threshold where the model accuracy levels off. A comprehensive study of the National Weather Service's wind predations for the gauge

locations needs to be conducted to fully understand the error, but Hu and Skaggs (2009) show that weather estimates can show strong regional variations. As weather prediction increases in accuracy so will the model's predictive strength.

Further improvements can be made in the accuracy assessment of the predictive model. Currently past data predictions are not available for each of the stations so a proper analysis of the predictive ability of the model is difficult to achieve. The model accuracy assessment for the predictive portion of the model is done by recording the National Weather Services' predictions in a database and subsequently comparing these predictions to actual measurements. This will require the accuracy assessment to run for a year or two to fully understand the impacts of weather prediction using point forecasts at each gauge. This will simply take time.

An addition to the model that could help boost overall accuracy would be to incorporate time duration of wind speed and direction. The change in water level when the wind shifts direction is not an instantaneous event but an event that occurs over time. When winds are sustained out of a given direction and are of a sufficient speed, water levels can surpass the ETM's prediction.

An attempt was made to incorporate into the model the duration at which a given wind speed was exhibited. A variable sized moving window analysis was conducted on the historic data looking for sustained periods of a single wind speed and direction. Once a range was identified the increase overtime in deviation of the observed water level from NOAA's predicted water level was examined. A rate of change per hour was calculated and entered into a separate matrix which was structured like the base model

matrix with wind speed on the x axis and wind direction on the y axis. To allow for slight variations in conditions, ranges of wind values were used and simplified directions were used (i.e. N, NNE, E, SSE, S, SSW, W, NNW). Wind direction could fluctuate by X and wind speed could fluctuate by Y before the moving window analysis decided that the conditions were no longer like the start conditions and the window was closed. The window was also limited by time. A time frame of less than 10 hours was not considered as shorter time frames could have too much stochasticity to obtain a reliable rate of change. Once this rate value was calculated and entered into the matrix the predictive program accessed the matrix and used the duration value to add to the (ETM-pred) value when the duration characteristic was met in the predicted wind conditions. No accuracy analysis was conducted as the method proved to need more development than time and money allowed, and the method was dropped from the model. Anecdotal observations of model performance showed that using 'Duration' aided in reducing underestimation of more extreme tidal events such as cold fronts. However, the relationship between water level and duration appears to be non-linear. The additive method that was implemented with the ETM produced estimates that would compound leading to large errors overtime. Limiting parameters needed to be implemented to control maximum and minimum rates in water level changes and the length of time the duration factor could be added. Basic attempts were made to test this at a few gauges in Galveston Bay and proved to be somewhat effective in limiting erroneous predictions, but each gauge in the gulf is different with different limiting factors. If duration could be implemented the ETM model's accuracy could be increased even more.

User-friendly Maps and ETM Output Graphics

An interactive, GIS-based Graphical User Interface (GUI) was created to display station results in map form (Figure 22 and 23) (Appelhans, Detsch, Reudenbach, and Woellauer, 2017). The GUI was constructed in .html format, and is ready to be hosted on the web and made accessible to the public. The latitude and longitude coordinates for each gauge location were gathered and compiled and a R programming function (mapview) was used to plot and link them (Appelhans, Detsch, Reudenbach, and Woellauer, 2017).

Each point can be clicked on and was linked to a pop-up window, displaying ETM predictions for that location. R programming was used to create this .png graphical plot (Urbanek, 2017) that included NOAA's prediction, the ETM prediction, and the observed tidal measurement. The location, wind speed and direction, time, and water level are all included in the graph as well.

These graphical pop-up window plots are stored in a figure repository that can be accessed individually by the program designer, or by the end user through the .html-based GUI. The graphs are flexible and can auto resize the y axis to allow for large changes in observed water level or time represented without the graph becoming hard to read. To produce all hourly graphs for 89 separate stations across the Gulf of Mexico, the average run time of ETM is approximately 15 minutes.

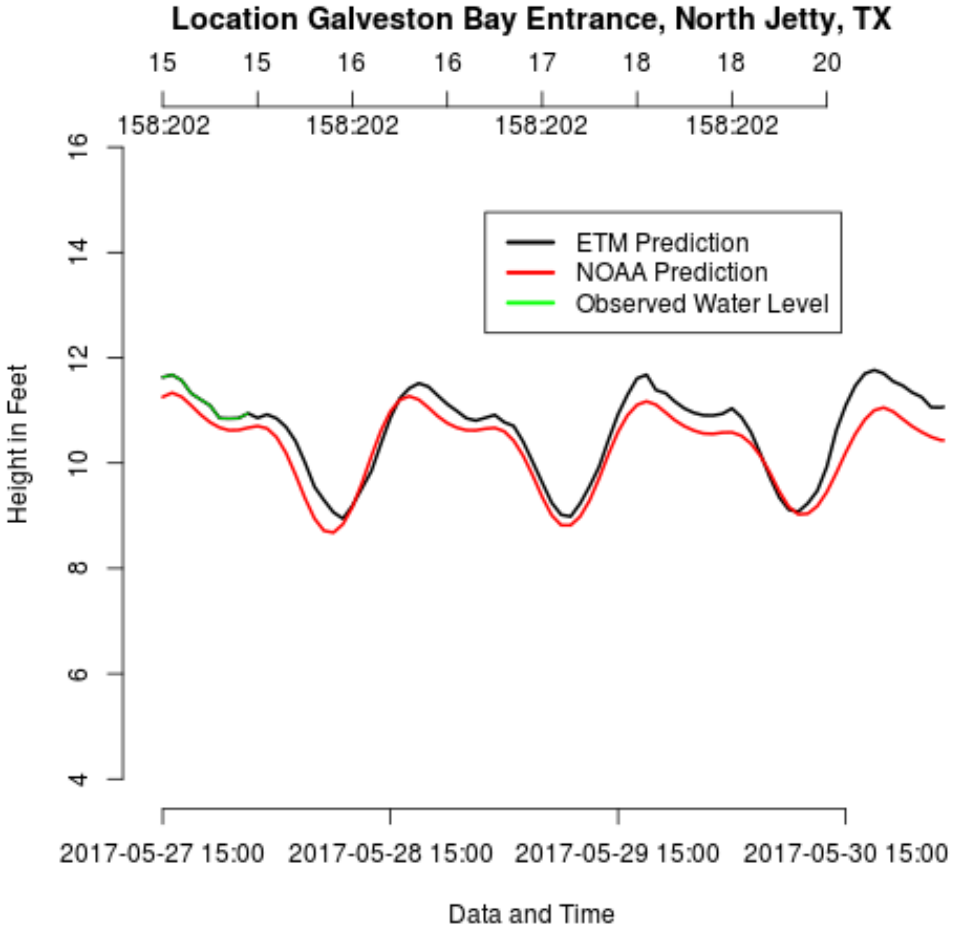

Figure 22: Graph of ETM tide prediction (black line), NOAA tide prediction (red line), and observed water level (green line). The top x axis denotes wind speed (top) and wind direction (bottom). This figure shows a close up of the graphs attached to the popup icons in the GUI map.

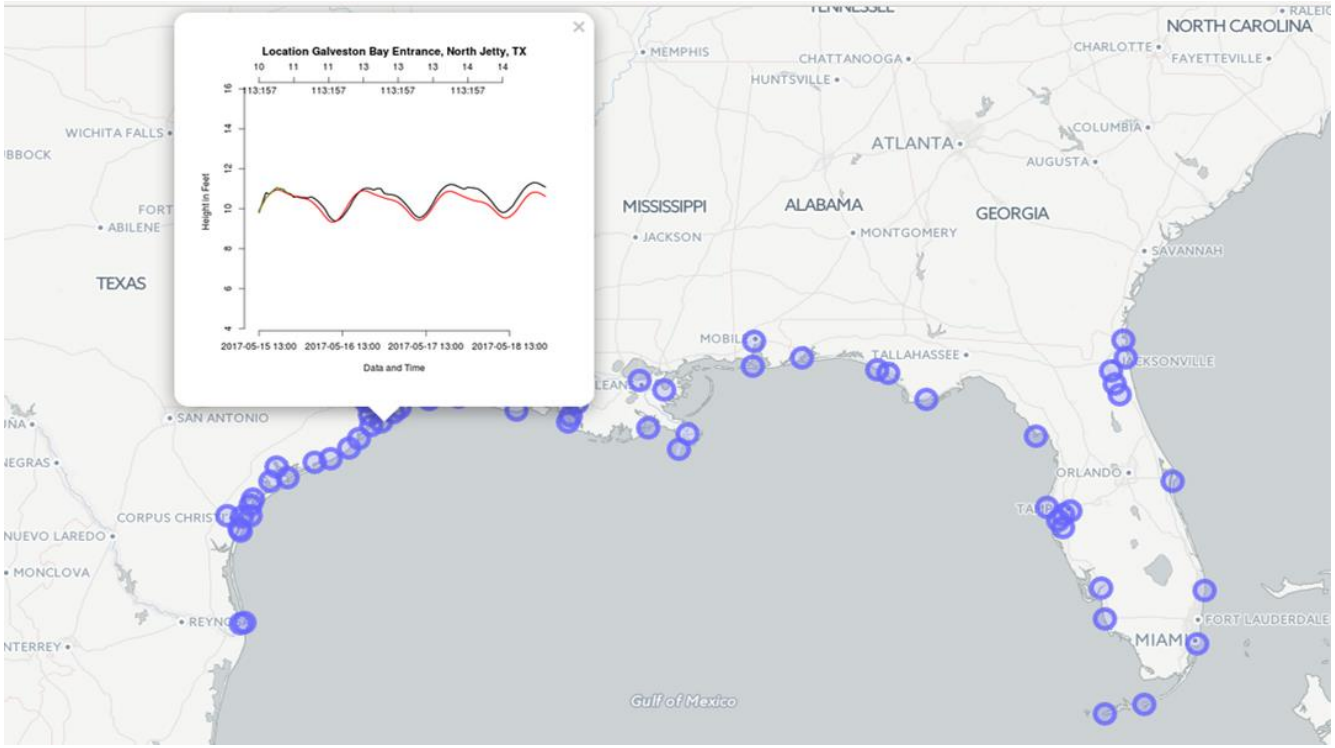

Figure 23: HTML GUI of gauge locations with popup graph of prediction. Red line is the Enhanced Tide Model, Black line indicates NOAA's estimate, and the Green line is the observed water level. The Blue circles on the map show each prediction location.

Conclusion

The ETM model possesses the potential to predict the tide level universally, as it simply requires empirical seed data, as opposed to a numerical or processed-based model that represents a single system. By using recorded data at each location, the model incorporates many stochastic factors such as inlet dynamics, gauge location, bathymetry, time, and local weather factors. This flexible model allows for a predictive model to be created in almost any location on earth that has a tide gauge, astronomical tide predictions, and wind data. The two-part structure of the ETM model (base and predictive) allows for its expansion to any location that has enough data to appropriately fill the base matrix. As new stations come on line, they can be incorporated after 20 months.

Public use of the ETM can enable the transportation and shipping industry to operate more safely in shallow waters, allow outdoor enthusiasts access to recreational fishing and hunting location at the appropriate portions of the tidal cycle, support the public use of boat ramps within more appropriate tolerance limits, enable infrastructure construction and ecological restoration operations to have advance notice of optimum water level working conditions, and improve the prediction of flood risk for coastal communities. We envision the ETM as a resource for industry and the public to make informed decisions that impact their livelihood.

CHAPTER V

CONCLUSIONS

This body of work demonstrates the importance of understanding tides when conducting hydrologic salt marsh restoration. The total area benefited by physical intervention in the Magnolia Beach marsh site was much larger than the amount of earth removed. Barrier removal as a form of hydrological restoration proves to be a very promising method and produces a high return on investment. By correcting the hydrology, the biotic and abiotic marsh systems will begin to recover. Little further human intervention is needed for continued success of the Magnolia Beach marsh.

The ETM also proved to be highly successful in predicting wind influenced tides in tidally connected waters. The potential exists for improvement of the model for even greater accuracy. Currently the model is already an effective tool to increase navigation safety, predict coastal flooding, and aid coastal restoration project planning. Adding wind duration estimates to increase accuracy and making this a web hosted product are also future goals.

The information obtained from this project will contribute to the knowledge of intertidal hydrology and marsh restoration, and allow for informed decision making by the public, government officials, and coastal managers.

REFERENCES

Adams, J. and Bate, G.C., 1995. Ecological implications of tolerance of salinity and inundation by Spartina maritima. *Aquatic Botany* ,52(3), 183-191.

Akima, H. and Gebhardt, A. (2016). akima: Interpolation of Irregularly and Regularly Spaced Data. R package version 0.6-2. https://CRAN.R-project.org/package=akima

Appelhans, T.; Detsch, F.; Reudenbach, C.; and Woellauer, S.; (2017). mapview: Interactive Viewing of Spatial Objects in R. R package version 2.0.1. https://CRAN.R-project.org/package=mapview

Boesch, D.F. and Turner, R.E., 1984. Dependence of fishery species on salt marshes: The role of food and refuge. *Estuaries*, 7(4), 460-468.

Bouma, T.J.; Belzen, J.V.; Balken, T., and Herman, P.M.J., 2014. Identifying knowledge gaps hampering application of intertidal habitats in coastal protection: Opportunities & steps to take. *Coastal Engineering*, 87, 147-157.

Broome, S.W.; Seneca, E.D., and Woodhouse Jr., W.W., 1988. Tidal salt marsh restoration. *Aquatic Botany*, 32(1), 1-22.

Bromber, G.K.; Silliman, B.R., and Bertness, M.D., 2009. Centuries of human-driven change in salt marsh. *Annual Review of Marine Science*, 1(1), 117-141.

Burkett, V. and Kusler, J., 2005. Climate Change: Potential impacts and interactions in wetlands of the United States. *Journal of the American Water Resources Association*, 36(1), 1-8.

Byrne, R.J.; Gammisch, R.A., and Thomas, G.R., 1980. Tidal prism-inlet area relations for small tidal inlets. *Proceedings of the 17th Coastal Engineering Conference, ASCE Press, NY*. 21(5), 2517-2533.

Cheng, R. T. and Smith, R. E. 1998. A Nowcast Model for Tides and Tidal Currents in San Francisco Bay, California. *Marine Technical Society*, p 537-543

Coast Guard News, 2015, Coast Guard oversees work to remove grounded tug, tank barge on Galveston Island, Texas. http://coastguardnews.com/coast-guard-oversees-work-to-remove-grounded-tug-tank-barge-on-galveston-island-texas/2015/10/26/

Colón-Rivera, R.J.; Feagin, R.; West, J.; Yeager, K., and Prairie, Y.T., 2012. Salt marsh connectivity and freshwater versus saltwater inflow: Multiple methods including tidal gauges, water isotopes, and LIDAR elevation models. *Canadian Journal of Fisheries and Aquatic Sciences*, 69(8), 1420-1432.

Costanza, R. d'Arge, R; de Groot, R.; Farber, S.; Grasso, M.; Hannon, B.; Limburg, K.; Naeem, S.; O'Neill, R. V.; Paruelo, J.; Raskin, R. G.; Sutton, P.; and van den Belt, M., 1997. The value of the worlds' ecosystem services and natural capital. *Nature*, 287, p 253-260.

Day, J.; Pont, D., Hensel, and P., Ibañez, C., 1995. Impacts of sea-level rise on deltas in the Gulf of Mexico and the Mediterranean: The importance of pulsing events to sustainability. *Estuaries*, 18(4), 636-647.

Delgado, P.; Hensel, P. F.; Swarth, C. W.; Ceroni, M., and Boumans, R., 2013. Sustainability of a tidal freshwater marsh exposed to a long-term hydrologic barrier and sea level rise. *Estuaries and Coasts*,36(3), 585-594.

Dunton, K.H.; Hardegree, B., and Whitledge, T.D., 2001. Response of estuarine marsh vegetation to intertidal variations to precipitation. *Estuaries*, 24(6), 851-861.

Feagin, R. A.; Figlus, J.; Zinnert, J. C.; Sigren, J.; Martinez, M. L.; Silva, R.; Smith, W. K.; Cox, D.; Young, D. R., and Carter, G. 2015. Going with the flow or against the grain? The promise of vegetation for protecting beaches, dunes, and barrier islands from erosion. *Frontiers in Ecology and the Environment*, 13(4), p 203-210.

Firtha, L.B.; Thompson, R.C.; Bohna, K.; Abbiatid, M.; Airoldid, L.; Boumae, T.J.; Bozzeda, F.; Ceccherelli, V.U.; Colangelod, M.A.; Evansa, A.; Ferrario, F.; Hanley, M.E.; Hinza, H.; Hoggart, S.P.G.; Jackson, J.E.; Moore, P.; Morgan, E.H.; Perkol-Finkel, S.; Skova, M.W.; Straind, E.M.; van Belzene, J., and Hawkins, S.J., 2014. Between a rock and a hard place: Environmental and engineering considerations when designing coastal defense structures. *Coastal Engineering*, 87(1), 122-135.

Hu, Q. S. and Skaggs, K.; 2009, Accuracy of 6-10 Day Predictions forecasts and Its improvement in the Past Six Years. Science and Technology Infusion Climate Bulletin. http://www.nws.noaa.gov/ost/climate/STIP/RServices/huq_032509.ht

Huff, T. and Feagin, R., 2017. Hydrological barriers as a cause of salt marsh loss. *Journal of Coastal Research, Special Issue:* In Revision.

Jackson, L. and Foote, Balistrieri, L., 1995. Hydrological, geomorphological, and chemical effects of hurricane Andrew on coastal marshes of Louisiana. *Journal of Coastal Research*, 21(1) 306-323.

Jarrett, J.T. 1976. Tidal Prism-Inlet Area Relationships. GITI Report 3. US Army Corps of Engineers, Coastal Engineering Research Center, Fort Belvoir, VA; US Army Corps of Engineers Waterways Experiment Station, Vicksburg, MS.

Kirwan, M.L.; Guntenspergen, G.R.; D'Alpaos, A.; Morris, J. T.; Mudd, S.M., and Temmerman, S., 2010. Limits on the adaptability of coastal marshes to rising sea level. *Geophysical Research Letters*, 37, 1-5.

Ko, J.Y. and Day, J.W., 2004. Wetlands: Impacts of energy development in the Mississippi delta. *Encyclopedia of Energy*, 6, 397-408.

Lefevre, F.; Le Provost, C.; Lyard, F. H.; 2000, How can we improve a global ocean tide model at a regional scale? A test on the Yellow Sea and the East China Sea.

Mathews, B.; Messter, L.D.; Jones, C.G.; Ibeling, B.W.; Bouma, T.J.; Nuutine, V.; Van De Koppel, J., and Odling-Smee, J., 2014. Under niche construction: An

operational bridge between ecology, evolution, and ecosystem science. *Ecological Monographs*, 84(12), 245-263.

Matsumoto, K, Takanezawa T, and Ooe M. 2000, Ocean Tide Model Developed by Assimilating TOPEX/POSEIDON Altimeter Data into Hydrodynamical Model: A Global Model and a Regional Model around Japan. *Journal of Oceanography*, p 56-567

Morris, J. T.; Sundareshwar, P. V.; Nietch, C. T.; KJerfve, B. and Cahoon, D. R. 2002, *Ecology*, 83(10) p 2869-2877.

Mukai, A. Y.; Westerink, J. J.; Luettich, R. A. Jr.; Mark, D. 2001. East Coast 2001, A Tidal Constituent Database for Western North Atlantic, Gulf of Mexico, and Caribbean Sea. *Defense Technical Information Center*.

Naidoo, G.; McKee, K.L., and Mendelssohn, I.A., 1992. Anatomical and metabolic responses to waterlogging and salinity in Spartina alterniflora and S. patens (Poaceae). *American Journal of Botany*, 79(7), 765-770.

NASA, ND, Ocean in Motion: Ekman Transport Background, http://oceanmotion.org/html/background/ocean-in-motion.htm, retrieved 5/1/2017

NOAA. 2016. National Centers for Environmental Information. Viewed Nov. 4, 2014 https://data.noaa.gov/dataset/u-s-hourly-precipitation-data

NOAA, 2016, Tides and Water Levels, accessed 5/20/2017. http://oceanservice.noaa.gov/education/tutorial_tides/tides09_monitor.html

NOAA, 2013. Our Restless Tides National Ocean Service, https://tidesandcurrents.noaa.gov/restles6.html

NOAA, 2010. Returning the Tide: A Tidal Hydrology Restoration Guidance Manual for the Southeastern United States. Silver Spring, Maryland: NOAA Restoration Center and NOAA Coastal Services Center, 96p.

NOAA, 2008, What Affects Tides in Addition to the Sun and Moon? http://oceanservice.noaa.gov/education/kits/tides/tides08_othereffects.html retrieved 1/13/2017

NOAA, 2001, Sea Level Variations of the United States 1854-1999. Technical report NOS CO-OPS 36

NWS. (2017), The National Weather Service Daily Forecast, accessed 5/25/2017, http://forecast.weather.gov

Portnoy, J. 1999. Salt marsh diking and restoration: biogeochemical implications of altered wetland hydrology. *Environmental Management,* 24(1), 111-120.

Powell, M.A.; Thieke, R.J., and Mehta, A.J., 2006. Morphodynamic relationships for ebb and flood delta volumes at Florida's entrances. *Ocean Dynamics,* 56(1), 295-307.

Roman, C.; Niering, W., and Warren, R 1984. Salt marsh vegetation change in response to tidal restriction. *Environmental Management,* 8(1), 141-150.

R Core Team (2017). R: A language and environment for statistical computing. R Foundation for Statistical Computing, Vienna, Austria. URL https://www.R-project.org/.

Roman, C.T.; Raposa, K.B.; Adamowicz, S.C.; James-Pirri, M., and Catena, J.G., 2002. Quantifying vegetation and nekton responses to tidal restoration of a New England salt marsh. *Restoration Ecology*, 10(3), 450-460.

Sinicrope, T.L.; Hine, P.G.; Warren, R.S., and Niering, W.A., 1990. Restoration of an impounded salt marsh in New England. *Estuaries*, 13(1), 25-30.

Stive, M.J.F., and Rakhorst, R.D. 2008. Review of the empirical relationships between inlet cross-section and tidal prism. *Journal of Water Resources and Environmental Engineering* 23(1) 89-95.

Temmerman, S; De Vries, M.B., and Bouma, T.J., 2012. Coastal marsh die-off and reduced attenuation of coastal floods: A model analysis. *Global and Planetary Change*, 92, 267-274.

Tiner, R., 1984. Wetlands of the United States: Current Status and Recent Trends. Washington DC: U.S. Fish and Wildlife Service National Wetlands Inventory, 59p.

Turner, R.F. and Neill, C., 1983. Revisiting impounded wetlands after 70 years. Water Quality and Wetland Management Conference Proceedings. (New Orleans, Louisiana), 309-322.

Urbanek, S. (2013). png: Read and write PNG images. R package version 0.1-7. https://CRAN.R-project.org/packag e=png

Warren, S.R.; Fell, P.E.; Rozsa, R; Brawley, A.H.; Orsted, A.C.; Olson, E.T.; Swamy, V., and Neiring, W.A., 2002. Salt marsh restoration in Connecticut: 20 years of science and management. *Restoration Ecology*, 10(3), 497-513.

White, W.A.; Tremblay, T.A.; Waldinger, R.L., and Calnan, T.R., 2006. Status and Trends of Wetland and Aquatic Habitat on Texas Barrier Islands Coastal Bend. Webster, Texas: Coastal Coordination Division, *Texas General Land Office*, 64p

Zavala-Hidalgo, J.; Morey, S. L.; O'Brien, J. J. 2003, Seasonal circulation on the western shelf of the Gulf of Mexico using a high-resolution numerical model. *Journal of Geophysical Research: Oceans*, 108(12).